Ph.D. Dissertation

Studies of the efficacy and mode of action of GPCR19 agonist (TDCA) in an Alzheimer's disease mouse model

알츠하이머 병 마우스 모델에서 GPCR19 작용제 (TDCA)의 효능 및 작용 기전 연구

August 2022

Graduate School of Medicine
Seoul National University
Biomedical Science Major

Md Jahirul Islam

Studies of the efficacy and mode of action of GPCR19 agonist (TDCA) in an Alzheimer's disease mouse model

Submitting a Ph.D. Dissertation of
Biomedical Science

April 2022

Graduate School of Medicine
Seoul National University
Biomedical Science Major

Md Jahirul Islam

Confirming the Ph.D. Dissertation written by
Md Jahirul Islam
July 2022

Chair _____(Seal)
Vice Chair _____(Seal)
Examiner _____(Seal)
Examiner _____(Seal)
Examiner _____(Seal)

Abstract

Alzheimer's disease (AD) is an inflammatory neurodegenerative disorder of the brain caused by accumulation of neuritic plaques and neurofibrillary tangles (NFTs). Neuroinflammation caused by Amyloid beta (Aβ) leads to neuronal apoptosis by activating various pro-inflammatory pathways such as NLRP3 inflammasome (N3I). We have investigated Taurodeoxycholate (TDCA), a G-protein coupled receptor 19 (GPCR19) agonist, inhibits neuroinflammation and neuronal degeneration.

Activation of NLRP3 inflammasome by way of P2X7R of microglia is crucial in neuroinflammation of Alzheimer's disease (AD). Damage-associated molecular patterns such as Amyloid β (Aβ) and/or ATP activates P2X7R pathway thereby N3I. GPCR19 is preferentially expressed on myeloid immune cells including microglia. We found that GPCR19 co-localized with P2X7R on the membrane of microglia and regulates P2X7R-mediated N3I activation. In 5x Familial Alzheimer's disease (5xFAD) mice, expression of GPCR19 and P2X7R changes upon aging. TDCA suppressed IL-1β production in WT mice but not in GPCR19KO and P2X7RKO microglia. Ca^{++} mobilization of microglial in response to ATP or BzATP was diminished in GPCR19KO and P2X7RKO cells when compared with WT cells, suggesting GPCR19 is crucial for P2X7R mediated N3I activation which is essential for production of IL-1β/IL-18. *In vitro*, TDCA suppressed NLRP3-ASC oligomerization and production of mature IL-1β/IL-18 in microglia cells by Aβ ± ATP. TDCA also inhibited the priming phase of N3I activation via GPCR19-cAMP-PKA-NF-kB pathway. Further, TDCA (1mpk, i.p., q.d. for 10 weeks) suppressed expression of P2X7R, enhanced phagocytosis of Aβ, and decreased number of Aβ plaque in the brain of 5xFAD mice. TDCA also reduced microgliosis, prevented neuronal loss, and improved memory function of 5xFAD mice.

After oral administration TDCA (30mpk, p.o, b.i.d. for 10 weeks), memory function of 5xFAD mice was improved as much as TDCA injected i.p. The $AUC_{(last)}$ of TDCA in plasma and brain is 3341.98 ng/ml and 2657.64 ng/ml respectively after single oral administration indicating the distribution of TDCA into the brain. The pleiotropic roles of GPCR19 in P2X7R-mediated N3I activation suggest that targeting GPCR19 might resolve neuroinflammation in AD patients.

*This dissertation is based on a previously published article (Islam et al., 2022).

Keywords: Taurodeoxycholate, GPCR19, P2X7R, Alzheimer's disease, Neuroinflammation, Inflammasome

Student Number: 2015-30886

Contents

List of Figures

List of Tables

Chapter 1. Introduction

Alzheimer's disease (AD) is a neurodegenerative disorder constituting the most common cause of dementia[1,] and the etiology is multifactorial[2]. AD patients show massive neuronal death in the hippocampus and cortex due to neuroinflammation caused by tau neurofibrillary tangles and amyloid-β (Aβ)[3,4]. For the last few decades, tau and Aβ plaques have been targeted for the treatment of AD patients without successful outcomes[5]. Despite Alzheimer's disease (AD) being the most common cause of dementia, no effective treatments are currently available[1]. Cholinergic, tau, and amyloid hypotheses have been suggested to explain the pathophysiology of AD[6]. Currently, the treatment choices for AD patients are mostly based on cholinergic neurotransmission, which cannot sufficiently mitigate the progression of AD[7]. Although glial cells constitute more brain cells than neurons, neurons have received more attention than glial cells for a long time, possibly due to the prominent neurological symptoms of AD patients[8]. Within the last few years, however, clinical trials have moved to reduce neuroinflammation induced by reactive microglia[9].

Neuroinflammation led by Aβ-activated microglia induces neuronal apoptosis in the hippocampus and cortex of AD patients[10]. In the brains of AD patients, proinflammatory mediators, such as reactive oxygen species (ROS), reactive nitrogen species (RNS), IL-1β, IL-6, and tumor necrosis factor (TNF)-α, are frequently increased[11]. The insoluble aggregates of Aβ and hyperphosphorylated tau, which make neurofibrillary tangles, are possibly the main initiators of neuroinflammation in these patients[12]. These damage-associated molecular patterns (DAMPs) interact with pattern recognition receptors (PRRs) on membranes of brain cells or in the cytosol to initiate proinflammatory pathways[13]. Sustained neuronal apoptosis may unleash more DAMPs in the brain, which further

amplifies sterile inflammation in the brain[14]. Considering that neuroinflammation plays crucial roles in cognitive and memory deficits by neuronal loss, controlling neuroinflammation may provide promising therapeutic strategies[15].

The inflammasome plays central roles in the pathogenesis of many inflammatory disorders, including AD[16]. The NACHT, LRR, and PYD domains-containing protein 3 (NLRP3) polymorphisms are closely related to AD incidence[17]. Among the several inflammasomes, the most crucial contributor in AD pathologies is NLRP3[18]. Aβ was efficiently cleared and cognition was improved in the AD mouse model by inhibiting activation of the NLRP3 inflammasome (N3I)[19], suggesting that N3I is crucial in inflammatory neurodegeneration of AD[20].

The PRRs, such as CD36, CD14, TLR2, RAGE, and P2X7, of microglia are crucial in Aβ-triggered activation of the NLRP1 inflammasome (N1I) and N3I[21], which causes IL-1β/IL-18/pyroptosis-mediated inflammation in mice and in AD patients[17]. Unfortunately, however, strategies targeting components of N3I have not been successful in clinical trials for AD until now[22]. This may be due to redundant proinflammatory pathways activated by Aβ. For example, several PRRs recognize cytoplasmic tau and extracellular Aβ. Furthermore, the inflammasome is activated by canonical and noncanonical pathways, consisting of pro-caspase-1/4/5/11, gasdermin D, ASC, NLR proteins (such as NLRP1, NLRP3, NLRC4, NLRP6, or NLRP12), absent in melanoma 2 (AIM2), IFN-inducible protein 16 (IF116), and pyrin[23,24], although their roles in Aβ-mediated inflammasomal activation have not yet been elucidated in detail. The significance of redundancy in developing inflammasomal inhibitors was well demonstrated in studies using the NLRP3-specific inhibitor MCC950[25]. MCC950 showed promising efficacy in preclinical settings but not in clinical settings[26]. The redundancy of inflammasomal activation pathways implies the evolutionary significance of the inflammasome responding to diverse environmental or endogenous threats to maintain tissue homeostasis[27]. For

these reasons, a molecule at a higher level of the inflammasomal signaling cascade requires regulation to overcome redundancy in inflammasomal activation. A more plausible approach may involve targeting P2X7R, which is one of the top regulators of the signaling cascade necessary for N3I activation[28].

Brain cells, including microglia, express purinergic receptors, and both ionotropic P2X and metabotropic P2Y receptors are crucial in AD pathogenesis[29]. P2X7R is the ion channel primarily studied in terms of N3I activation by Aβ[30]. Upon binding with ATP or Aβ, P2X7R renders cell membranes permeable to K^+ and Ca^{++}, which activate the inflammasome[31]. N3I of $P2X7R^{-/-}$ microglia was not activated in response to Aβ[32], suggesting the essential role of P2X7R in Aβ-mediated neuroinflammation. P2X7R promotes the assembly of N3I, secretion of IL1β/18, and pyroptosis[33]. Intriguingly, P2X7R is overexpressed in glial cells from AD patients, and Aβ injection into the hippocampus increases P2X7R expression[34]. Taken together, P2X7R plays a key role in chronic neuroinflammation and neurodegeneration in AD.

Apyrase blocks the activation of N3I by Aβ[35], suggesting that the ATP-P2X7R interaction is crucial in N3I activation in response to Aβ[36]. High levels of ATP are passively released from necrotic cells and act as proinflammatory DAMPs, binding to P2X7R and activating N3I[37]. P2X7R activation creates membrane pores through which ATP can leak further[38].

Activation of P2X7R is also crucial in impairing phagocytosis of Aβ[39]. In AD patients, the phagocytic ability of microglia was insufficient to clear Aβ[9]. $P2X7R^{-/-}$ microglia phagocytosed Aβ more efficiently than wild-type microglia[40]. These findings clearly show both proinflammatory roles and antiphagocytic functions of P2X7R in glial cells[41].

Thus, many P2X7R inhibitors have been developed to control inflammasomal activation without success until now[42]. These inhibitors effectively decreased

inflammatory responses in AD mice[43]. However, many of these did not meet the clinical needs[44]. Human P2X7R is highly polymorphic, and there are several isotypes[45]. Ten human P2X7R gene splice variants (P2X7RA–J) might produce a complex combination of P2X7R with various haplotypes that cause a broad spectrum of responsiveness to P2X7R inhibitors in clinical settings.

Bile acids (BAs) are evolutionally conserved molecules synthesized in the liver that regulate a variety of metabolic functions by modulating nuclear and membrane receptors. Farnesoid X receptor (FXR), pregnane X receptor (PXR), constitutive androstane receptor (CAR), vitamin D receptor (VDR), liver X receptors α/β (LXRα/β), and RAR-related orphan receptor γt (RORγt) are nuclear receptors for bile acids[46]. G protein couple receptor 19 (GPCR19) also known G protein-coupled bile acid receptor 1 (GPBAR1), membrane-type receptor for bile acids (M-BAR) or Takeda G protein-coupled receptor 5 (TGR5) is one of membrane receptor for bile acid. Nuclear receptors of bile acids are a group of ligand-activated transcription factors. Upon ligand binding and activation, nuclear receptors regulate the transcription of genes involved in various biological processes, ranging from development, differentiation, and metabolism[47].

Bile acids (BAs) are derived from cholesterol. Cholic acid (CA) and chenodeoxycholic acid (CDCA) are the two most common types of primary bile acids, which are synthesized in the liver and conjugated to either taurine or glycine. The conjugated primary bile acids are known as glycocholic acid, taurocholic acid, glycochenodeoxycholic acid (GDCA), and taurochenodeoxycholic acid (TDCA). The most common secondary bile acids—deoxycholic acid (DCA) and lithocholic acid (LCA)—are synthesized by microbial flora of the small intestine. These two bile acids are produced by deconjugation and dehydroxylation of primary bile acids. The cytotoxicity of bile acids is dependent on their structural formation, while their hydrophobicity is based on the number and position of the hydroxyl group in the

ring structure. Chemical structure of different bile acids[48]:

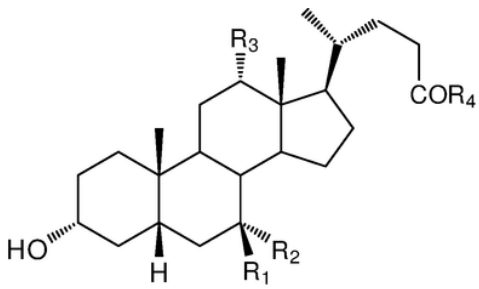

Bile acids	R_1	R_2	R_3	R_4
CA	H	OH	OH	OH
GCA	H	OH	OH	$NHCH_2COOH$
TCA	H	OH	OH	$NH(CH_2)_2SO_3H$
CDCA	H	OH	H	OH
GCDCA	H	OH	H	$NHCH_2COOH$
TCDCA	H	OH	H	$NH(CH_2)_2SO_3H$
DCA	H	H	OH	OH
GDCA	H	H	OH	$NHCH_2COOH$
TDCA	H	H	OH	$NH(CH_2)_2SO_3H$
UDCA	OH	H	H	OH
GUDCA	OH	H	H	$NHCH_2COOH$
TUDCA	OH	H	H	$NH(CH_2)_2SO_3H$
LCA	H	H	H	OH
GLCA	H	H	H	$NHCH_2COOH$
TLCA	H	H	H	$NH(CH_2)_2SO_3H$

In addition to metabolic homeostasis, various bile acids play pivotal roles in modulating inflammation[49]. For example, different GPCR19 agonists inhibit inflammation of the stomach[50] and brain[51]. Deoxycholic acid (DCA) and lithocholic acid (LCA) are the physiological ligands of GPCR19[52]. Additional metabolism of secondary bile acid DCA and LCA can form UDCA (ursodeoxycholic acid) and TLCA (Taurolithocholic acid) respectively[53]. UDCA is considered as safe and effective treatment for cholestatic liver disease. Studies have shown that UDCA can effectively activate GPCR19 and play a beneficial role in a NASH mouse model. However, The EC_{50} of UDCA is 14 μM, which is 4–7 times higher than the TLCA EC_{50}[54]. TUDCA is a taurine conjugate derivative of UDCA that is offen used in the treatment of gallstones and chronic cholestatic liver disease[55]. TUDCA can also activate GPCR19 and induce an increase in the level of cAMP in microglia, subsequently exerting an anti-inflammatory effect[56].

Semisynthetic BA derivatives like INT-777 is a specific GPCR19 agonist that can reduce neuroinflammation, improve cognitive impairment, improve glucose tolerance, and increase insulin synthesis[57,58]. In addition, INT-777 induces the release of GLP-1 from enteroendocrine L-cells, which can improve liver and pancreatic function in mice, stimulate bile flow, and inhibit macrophage inflammation[59,60]. In addition to INT-777, a small molecular agonist of GPCR19, BAR501 has been shown to regulate the M1/M2 phenotype of intestinal macrophages and effectively reduce the expression of inflammatory factors[61].

Activation of GPCR19 attenuates caspase-8/NLRP3-mediated neuroinflammation in rats[62]. For these reasons, a nonpolymorphic physiological regulator for P2X7R might be an alternative target to control inflammasome activation. We have observed the colocalization of G protein coupled protein 19 and ion channel P2X7R in microglia. P2X7R receptor is an upstream sensor for the activation of NLRP3 inflammasome. When we found reduced Ca2+ mobilization in microglia from GPCR19KO mice and P2X7RKO mice compared to WT (C57BL/6) mice, we then hypothesized that controlling P2X7R by GPCR19R ligand can suppress the NLRP3 inflammasome and subsequent secretion of pro-inflammatory cytokine IL-1β and IL-18, which leads us to use a GPCR19 agonist (TDCA) to suppress the NLRP3 inflammasome activation in an inflammatory disease like Alzheimer's diseases. We found that GPCR19 regulates P2X7R in N3I activation. TDCA, a GPCR19 agonist, inhibited the priming phase of N3I activation of microglia by activating adenylate cyclase, as reported earlier in other types of cells, and inhibited the activation phase of N3I by inhibiting P2X7R function.

Method and Materials

Human brain samples

A total of eight postmortem brain samples were obtained (Supplementary Table 1); five from individuals with clinically and neuropathologically diagnosed AD (Braak stages: V–VI) and three from nondemented controls. Brain sections were provided by the Korea Brain Bank Network (KBBN) operated through the National Brain Bank Project funded by the Ministry of Science and ICT. The project was approved by the Scientific Committee of the Brain Bank.

Reagents

TDCA was purchased from New Zealand Pharmaceuticals Ltd. (Palmerston North, New Zealand). KH7 (Ann Arbor, Michigan, USA) was dissolved in DMSO. ATP and BzATP (Sigma–Aldrich, St. Louis, MO, USA) were dissolved in PBS. INT777 (MedChemExpress, NJ USA), MCC950 (InvivoGen, San Diego, California, USA), A 740003 (TOCRIS, Bristol UK), GW 791343 (TOCRIS, Bristol UK) were dissolved in DMSO.

Preparation of the $A\beta_{1\text{-}42}$ oligomer

A lyophilized 0.1 mg vial of amyloid β protein fragments 1-42 (Aβ; Sigma–Aldrich) was dissolved in 50 µl DMSO (Sigma–Aldrich) for 1 h at room temperature with continuous rotation. Oligomeric $A\beta_{1\text{-}42}$ was prepared by diluting the dissolved Aβ to 100 µM using DMEM/F12 media. The resulting solution was then incubated for 24 h at 4 °C with continuous rotation.

Isolation of Primary Microglia and Culture

Primary microglia were obtained from the cerebral cortices and hippocampi of male and female 1- to 2-day-old B6 mice or adult B6, $GPCR19^{-/-}$, and $P2X7R^{-/-}$ mice (Jackson Laboratory, USA) using a mouse brain dissociation kit (Miltenyi Biotec

GmbH, Bergisch, Gladbach, Germany). The tissue was cut into fragments using a scalpel blade (Medicom, Los Angeles, CA, USA) and then homogenized using a gentleMACS(TM) C tube and gentleMACSTM Octo Dissociator (Miltenyi Biotec GmbH). Single-cell suspensions were obtained after passing the tissue homogenates through MACSR Smart Strainers (70 µm; Miltenyi Biotec GmbH). The myelin was depleted using a debris removal solution supplied with the kit. Microglial cells were isolated using CD11b MicroBeads, LS Columns, and a MACS multistand system (all obtained from Miltenyi Biotec GmbH). Isolated microglia were washed with PB buffer (0.5% FBS in PBS) and cultured using DMEM-F12 media with 20% FBS and 10 ng/ml M-CSF (PeproTech, Rocky Hill, NJ) in a 95% air and 5% CO2 atmosphere at 37 °C.

For inflammasome activation, primary microglial cells from 1- to 2-day-old B6 mice were seeded on 12-mm microscope cover glasses (Deckglaser, Luda-Konlgshofen, Germany) in 24-well PDL-coated cell culture plates (Corning, Wujiang, Jiangsu, China) at 7.5 x 10^4 cells/ml per well for 24 h, serum starved for 10 h and treated with Aβ (2 µM), TDCA (400 ng/ml) for 24 h, and ATP (1 mM) for the final hour.

Cell culture

BV2 cells (Murin microglial cell line) were maintained in a 95% air and 5% CO_2 atmosphere at 37 °C in DMEM (Dulbecco's modified Eagle's medium complete media; Invitrogen, Carlsbad, CA, USA) containing 10% FBS (Fetal Bovine Serum; Invitrogen) and 1% penicillin and streptomycin (Invitrogen). BV2 cells were seeded in 6-well (1.5 x 10^5 cells/2 ml), 12-well (1 x 10^5 cells/ml), or 24-well (5 x 10^4 cells/0.5 ml) PDL-coated cell culture plates for 12 h using DMEM complete media. Cells were serum starved before treatment for 10 h using DMEM/F12 media (Thermo Fisher Scientific, Waltham, MA, USA). Cells were treated with Aβ (2 µM), TDCA (400 ng/ml), and ATP (1 mM) for 1 h in the case of GPCR-19–P2X7R interaction. For inflammasome activation and inhibitor (KH7) assays, cells were

treated with Aβ (2 μM), KH7 (4 μM), TDCA (400 ng/ml) for 24 h, and ATP (1 mM) for the final hour. DMEM/F12 medium was used unless stated otherwise. The cell-lysed supernatants were used to check the concentrations of cAMP, and cell culture supernatants were used to analyze the concentrations of IL-1β, IL-18, TNF-α, and caspase-1 using ELISA.

Measurement of microglial Ca^{++} response

Adult mouse microglial cells isolated from adult B6, GPCR19$^{-/-}$, and P2X7R$^{-/-}$ mice were seeded on 25-mm cover glasses (Deckglaser) in a 6-well plate. After 48 h of culture with DMEM/F12 medium containing 20% FBS and 10 ng/ml M-CSF in a 95% air and 5% CO_2 atmosphere at 37 °C, cells with glass coverslips were transferred and loaded with 2 μM Fluo-4/AM for 30 min at 37 °C in a physiological external solution consisting of 138 mM NaCl, 5.6 mM KCl, 0.5 mM MgCl2, 2 mM CaCl2, 10 mM HEPES, and 10 mM glucose (pH 7.4). After loading, cells on the coverslips were transferred to an open perfusion chamber, and fluorescence was measured at 494/506 nm using a fluorescence microscope (Nikon, Tokyo, Japan). The microscope was equipped with an LED lamp (Andover, UK), integrated shutter, and cooled EM-CCD camera. The camera and shutter were controlled using MetaMorph software (Molecular Devices, Foster City, CA). Single cells were defined as regions of interest (ROIs). Sixteen-bit grayscale images with a binning of 1 x 1 were captured every 1 s with a ranging exposure time. Data were processed using OriginPro 8 software (OriginLab) and merged from three independent experiments.

BV2 cells were seeded on 25-mm cover glasses in a 6-well plate. After starvation, cells were treated with Aβ (2 μM) with or without TDCA (400 ng/ml) for 24 h. Cells with glass coverslips were transferred and loaded with 2 μM Fluo-4/AM for 30 min at 37 °C in the physiological external solution mentioned above. After loading, the cells were transferred to an open perfusion chamber, and fluorescence was

measured at 494/506 nm as previously described.

BV2 cell Ca^{++} sensing was measured using a BD calcium assay kit (BD Bioscience, San Diego, CA, USA) according to the manufacturer's protocol. In a 6-well plate, 1.5 x 10^5 cells/2 ml media were treated with Aβ with or without TDCA for 24 h after serum starvation. Cells were harvested from the cell culture plate in a FACS tube, washed with complete RPMI media, loaded with loading dye, and incubated for 1 h at 37 °C in a 5% CO_2 atmosphere. Cells were acquired for 1 min for basal signaling, incubated with BzATP (300 μM) for 2 min, and recorded for an additional 4 min using flow cytometry (LSRFortessa, BD Biosciences, San Jose, CA, USA). Relative fluorescent units (RFUs) were calculated using FlowJo version 9.0 (Treestar, Ashland, OR, USA).

Immunoblot

Cortices were harvested from 3 sets of B6 (3-month-old) and 5xFAD (3-, 4-, 6-, and 9-month-old) mice, lysed with RIPA buffer (Thermo Fisher Scientific, Meridian Road, Rockford, USA) supplemented with phosphatase inhibitor cocktail 2 (Sigma–Aldrich), and centrifuged to remove cell debris. The concentrations of the prepared protein samples were determined using a BCA kit (Thermo Fisher Scientific). Protein samples were separated by electrophoresis on 10% sodium dodecyl sulfate–polyacrylamide gels and then transferred electrophoretically to immobilon, polyvinylidene-difluoride membranes (Merck, Millipore, Billerica, MA, USA). The membranes were incubated at 4 °C overnight with anti-GPCR19 polyclonal antibody (Novus Biologicals, Littleton, CO, USA), P2X7R monoclonal antibody (Clone 1F11, Biolegend, San Diego, CA, USA), and anti-β-actin (Sigma–Aldrich). The following day, the membranes were washed and then incubated with horseradish peroxidase-labeled anti-rabbit or anti-mouse secondary antibodies for 1 h at room temperature. Subsequently, membrane-bound horseradish peroxidase-labeled antibodies were detected using an enhanced

chemiluminescence detection system, including the Pierce ECL Western Blotting Substrate kit (Thermo Fisher Scientific). Densitometric quantification of the bands was conducted using ImageJ software (Rasband, W.S., NIH, Maryland, USA). Protein levels were normalized to β-actin for quantification.

Immunocytochemistry

BV2 cells or primary microglial cells isolated from adult mouse brains were seeded on 12-mm microscope cover glasses (Deckglaser) in 24-well plates. Cells were stained with anti-GPCR19 polyclonal antibody (Novus Biologicals) and P2X7R (Clone 1F11, Biolegend) at 4 °C overnight, followed by staining with goat anti-rabbit IgG, Alexa Fluor 488 (Thermo Fisher Scientific), and goat anti-rat IgG, Alexa Fluor 546 (Invitrogen) for 1 h at RT.

To stain for inflammatory components, primary microglial cells isolated from the brains of 1- to 2-day-old B6 mice were seeded on 12-mm microscope cover glasses in 24-well plates and treated with Aβ (2 μM), TDCA (400 ng/ml) for 24 h, and ATP (1 mM) for the final hour. The cells were permeabilized and stained with anti-NLRP3 polyclonal antibody (Abcam, Cambridge, United Kingdom) and anti-ASC antibody (Clone B-3, Santa Cruz Biotechnology, Inc. Dallas, Texas, USA) at 4 °C overnight, followed by staining with secondary polyclonal antibodies, Alexa Flour 488-labeled goat anti-rabbit IgG, or Alexa Flour 532-labeled goat anti-mouse IgG (Invitrogen) for 1 h at RT.

After rinsing with secondary polyclonal antibodies, cover glasses were placed on DAPI mounting solution (Vector laboratories, Burlingame, CA, USA) on glass slides. Fluorescence imaging was performed using a Confocal Microscope A1 (Nikon, ECLIPSE Ti, New York, USA). The colocalization percentage of NLRP3-ASC was measured using ImageJ software after setting the color threshold caliper to only yellow. NIS-Elements.AR. Ink (version 4.2, Nikon) was used to measure the mean fluorescence intensity (MFI) of the ROIs.

Quantitative RT–PCR

Tissue or cells were harvested after treatment, and total RNA was isolated using an RNeasy Plus Mini kit (QIAGEN, Hilden, Germany). cDNA was prepared from 1 μg of total RNA using a Maxime RT PreMix kit (iNtRON Biotechnology, Gyeonggi-do, South Korea). Thereafter, real-time quantitative PCR (qPCR) was performed using SYBR Green Fast mix (Applied Biosystems, Woolston, Warrington, UK) and primers specific to target genes (Supplementary Table 2) in the StepOnePlus™ Real-Time PCR system (Applied Biosystems, Marsiling Industrial Estate Road, Singapore). The expression levels of target mRNAs were analyzed using the ddCt method and were normalized to the expression levels of mouse *GAPDH*, a housekeeping gene used as an endogenous control. All fold changes are expressed relative to the control group.

ELISA

Cell-secreted cytokines were measured from the cell culture supernatant using commercially available ELISA kits for mouse TNF-α, IL-1β/IL-1F2 (R&D Systems, Minneapolis, MN, USA), IL-18 (MBL, Naka-Ku, Nagoya Aichi, Japan), and Caspase-1 (Novus Biologicals) according to the manufacturer's protocols. BV2 cells were cultured in the presence of Aβ (2 μM), TDCA (400 ng/ml), or KH7 (4 μM) for 24 h. Cells were harvested and lysed with 0.1 M HCl to measure intracellular cAMP using a cAMP assay kit (Abcam) according to the manufacturer's protocol.

Measurement of ROS production

BV2 cells were harvested in a FACS tube after treatment with Aβ (1~4 μM) and TDCA (400 ng/ml) for 24 h. Cells were washed with DPBS and incubated with 5 μM 2′-7′-dichlorofluorescin diacetate (Invitrogen, Eugene, Oregon, US) in DMEM containing 1% penicillin and streptomycin for 30 min at room temperature in the dark. Samples were washed in DPBS, suspended in FACS buffer containing DAPI

(0.3 μg/ml), immediately acquired and analyzed using a BD LSR Fortessa flow cytometer (BD Bioscience, San Jose, CA, USA) and FlowJo v9 software.

Phagocytosis of fAβ oligomer

Primary microglia isolated from 1- to 2-day-old B6 mice were cultured, pretreated with TDCA (400 ng/ml) for 12 h, and then incubated with fAβ (1–42) oligomer (green) for 3 h. After incubation with fAβ, the cells were washed with ice-cold PBS and fixed with 4% paraformaldehyde (PFA). After blocking, the cells were incubated at 4 °C overnight with a primary antibody against P2X7R (BioLegend) or control IgG. The cells were then rinsed and incubated with goat anti-mouse IgG (H+L) secondary antibody (Invitrogen) for 1 h at room temperature in the dark. After rinsing, cover glasses were placed on the DAPI mounting solution on the glass slides. Fluorescence imaging was performed using a confocal microscope A1. NIS-Elements.AR. Ink (version 4.2, Nikon) was used to measure the MFI of ROIs.

BV2 cells were seeded on microscope cover glasses in 24-well plates for confocal microscopy. Cells were treated with or without TDCA for 12 h. HilyteFluor™ 488-labeled Aβ (1-42; AnaSpec, Freemont, CA, USA) was used for fAβ oligomers, as mentioned above. After pretreatment with TDCA, the cells were incubated with fAβ oligomers for 3 h, fixed with 4% paraformaldehyde (PFA), and permeabilized with 0.3% Triton X-100. After blocking, the cells were incubated at 4 °C overnight with primary antibody for LAMP2 (Clone M3/84, BD Pharmingen Inc., San Jose, CA, USA) or control rat IgG. After rinsing, the cells were incubated with goat anti-rat IgG Alexa Fluor 546 (Invitrogen) for 1 h at room temperature in the dark. After rinsing, cover glasses were placed on the DAPI mounting solution on the glass slides. Fluorescence imaging was performed using a confocal microscope A1. The colocalization percentage of fAβ-LAMP2 was measured using ImageJ software after setting the color threshold caliper to only yellow.

Animals

The 5xFAD mice co-overexpress high levels of APP with three FAD mutations (Swedish (K670N/M671L), Florida (I716V), and London (V717I)) and high levels of presenilin 1 (PSEN1) with two FAD mutations (M146L, L286V), which are specifically overexpressed in the brain and regulated by the neural-specific Thy1 promoter.[63] 5xFAD mice were maintained by breeding male 5xFAD mice with female B6 mice. The SJL F1 hybrid was produced by an SJL male and a B6 female. PCR was performed to genotype the mice. 5xFAD or SJL mice were kindly provided by Professor Mook-Jung, In-hee or Professor Sung, Jung-Joon, respectively, of Seoul National University. GPCR19$^{-/-}$ mice (C57BL/6-Gpbar1$^{tm1(KOMP)Vlcg}$ mice) and P2X7R$^{-/-}$ mice (C57BL/6. 129P2-P2rx7^{tm1Gab}/J) used in this study were purchased from Jackson Laboratory. All animal experiments were approved by the institutional animal care and use committees (IACUC) of Seoul National University (SNU-170517-25) and performed in accordance with animal ethics regulations. Mice were maintained in specific pathogen-free conditions at the animal facility of the Wide River Institute of Immunology.

Morris water maze test

Male and female 5xFAD mice (8 to 10 weeks old) were injected intraperitoneally (i.p.) with either 1 mg/kg TDCA or PBS five times/week for 10 weeks. Age- and gender-matched nontransgenic littermates were used as a control group. Behavioral tests were performed after treatment, and then mice were sacrificed for further experimentation.

The maze was composed of a circular pool (1.5 m in diameter, 80 cm in height) with spatial cues at three different locations. Before testing, the pool was filled with opaque water adjusted to 20 ± 1 °C. On the first day, mice were allowed to freely swim in the water for 60 sec to find the escape platform located in one quadrant of the pool. When the mice failed to find the platform, they were guided to the platform. Once on the platform, mice were allowed to remain there for 30 sec. From the next

day for 4 consecutive days, the same procedure was repeated from three different starting points to train the mouse, and the time to reach the platform was recorded every day. After the 4-day training period, the probe test was performed in the same manner but without the platform. Each mouse was allowed to swim from one starting point for 60 sec, which was recorded using a video camera. The video was analyzed for the movement of mice in the water using tracking software (SMART3.0, Panlab Harvard Apparatus, Barcelona, Spain) to count the number of crossings and the time on the platform and to measure the time spent in each quadrant of the pool.

Y-maze test

Mouse functional behavior tests were performed on TDCA- or PBS-treated 5xFAD mice and WT (B6) control mice. The Y-maze test was assessed over the course of four days. On the first 2 days, individual mice were habituated to the task room and experimenter for 5 min. On the third day, after the task room and experimenter habituation, mice were allowed to habituate to the Y-maze for less than 1 min. On the last day, mice entered the middle of the Y-maze and were allowed to move freely within the maze for 8 min. Each mouse movement was recorded using a video camera. The video was analyzed for all mouse entries regarding limbs that pass through each half arm of the maze. Total arm entries and the percentage of alteration were counted for each mouse and compared between groups of mice.

Novel object recognition test (NORT)

NORT was assessed over the course of 4 days. The apparatus consisted of a white acrylic box (350 mm x 450 mm x 250 mm). The basement of the box was divided into six equal rectangles. On the first 2 days, each mouse was habituated to the box for 10 min. On the third day, two similar cylindrical objects were fixed in the box, and mice were allowed to explore the objects freely for 10 min. On the last day, one cylindrical object was replaced by a similarly sized object, and the mouse

explored this for 5 min. Exploration of two cylindrical objects on the third day and exploration of the novel object and cylindrical object on day 4 were recorded for each mouse using a video camera. The total time and frequency of novel and old object exploration were counted for each mouse using video footage. The percent discrimination index of the novel object was calculated from the exploration time of novel and old objects.

Immunohistochemistry

Human samples of brain paraffin tissue sections (4 μM) from KBBN were used for cell surface GPCR19 and P2X7R expression. Tissue sections were deparaffinized in xylene and rehydrated in a graded ethanol series (100%, 90%, 80%, and 70%). Antigen unmasking was performed by heating the brain sections in citrate-based buffer (pH 6, Vector laboratories, Burlingame, CA, USA). The sections were blocked with a blocking solution of 10% normal donkey serum (Thermo Fisher Scientific) and 1% BSA in PBS for 1 h. Tissue samples were incubated overnight at 4 °C with GPCR19 (Novus Biologicals) and P2X7R (Novus Biologicals) primary antibodies. Slices were subsequently incubated for 1 h at room temperature with Donkey anti-Rabbit Alexa 488 (Invitrogen) or Donkey anti-Goat Alexa 555-conjugated (Invitrogen) IgG secondary antibodies and then counterstained with DAPI for 10 min.

TDCA- or PBS-treated 5xFAD or B6 mice were anesthetized and perfused with ice-cold PBS. Brains were harvested and maintained in 10% neutral buffer formalin (Sigma–Aldrich) for 24 h at 4 °C and then embedded in paraffin (Lecia, Illinois, USA). The paraffin-embedded brains were cut (3 μM) using a microtome (Thermo Fisher Scientific), deparaffinized in xylene, and rehydrated in a graded ethanol series (100%, 90%, 80%, and 70%). Antigen unmasking was performed by heating the brain sections in citrate-based buffer (pH 6, Vector laboratories, Burlingame, CA, USA). The sections were incubated in 0.3% Triton X-100 for 30 min at room

temperature for intracellular staining and then blocked with a blocking solution of 10% normal goat serum (Thermo Fisher Scientific) and 1% BSA in PBS for 1 h. Tissue samples were incubated overnight at 4 °C with the following primary antibodies: GPCR19 (Novus Biologicals), P2X7R (Clone 1F11, Biolegend), NLRP3 (Abcam), ASC (Santa Cruz Biotechnology), NeuN (Clone A60, Merck Millipore, Temecula, CA, USA), and GFAP (Thermo Fisher Scientific). Slices were subsequently incubated for 1 h at room temperature with Alexa 488-, 532-, or 546-conjugated IgG secondary antibodies, as appropriate, and then counterstained with DAPI for 10 min.

For apoptotic cell (Tunnel+) detection, frozen tissue sections from TDCA- or PBS-treated 5xFAD mice were fixed using 4% neutral buffer formalin in TBS for 20 min at RT. After washing, the TBS slides were incubated with 0.1% Triton X-100 for 3 min. The TUNEL assay was performed according to the manufacturer's instructions (Roche, In Situ Cell Death Detection TMR, red) and then counterstained with DAPI. For Iba-1 (Wako, Osaka, Japan) staining, a frozen section was prepared from a separate group of TDCA- or PBS-treated 5xFAD or B6 mice. Perfused brains were cryopreserved in a phosphate-buffered 30% sucrose solution for 24 h. The brains were then frozen on dry ice, cut on a cryostat into sequential 3 μm sections, and stored at −80 °C until processed for analysis.

The Aβ core plaque was labeled by treating brain tissues with 1% thioflavin-S (Sigma–Aldrich) in PBS for 10 min at room temperature after being deparaffinized in xylene and rehydrated in a graded ethanol series (100%, 90%, 80%, and 70%). The tissue slides were then washed three times with 70% ethanol following DW three times. Fluorescence imaging was performed using a Confocal Microscope A1 (Nikon). NIS-Elements.AR. Ink (version 4.2, Nikon) was used to measure the MFI of the ROI.

Global protein profiling

Anesthetized mice were perfused with cold PBS, and the whole brain was extracted, followed by snap-freezing using liquid nitrogen. The frontal cortex and hippocampus region of each mouse were collected and digested using urea- (8 M) based in-solution digestion. After protein quantification using the BCA assay (Micro BCA Protein Assay Kit, Thermo Fisher Scientific, Bremen, Germany), samples were pooled together group by group, and 300 µg of tissue extracts per group was separated via high pH reversed-phase fractionation using an Agilent 1260 HPLC infinity purification system (Agilent Technology, Santa Clara, CA, USA). The fractionated peptide samples were subsequently loaded onto traps (C18, 3 µm, 0.7 cm, Thermo Fisher Scientific) and EASY-Spray columns (C18, 2 µm, 100 Å, 50 cm, Thermo Fisher Scientific). Easy nano II Ultra Performance Liquid Chromatography and Q-Exactive Mass Spectrometry systems (Thermo Fisher Scientific) were used to separate the peptides. For Q-Exactive, a top 10 method was used. The Orbitrap mass analyzer was used to acquire full MS scans (m/z 300–1,600 range; resolution, 70,000). The Trans Proteomic Pipeline (Seattle Proteomic Center, Seattle, WA, USA) was used to convert the mass data files into mzXML files. Peptide masses were searched using a concatenated forward and reverse mouse international protein index (IPI) database (Decoy ipi.MOUSE.v3.80 database, 54285 entries)[64] with the SEQUEST-Sorcerer platform (Thermo Fisher Scientific, Sage-N Research, Milpitas, CA). Sorcerer (Sage-N Research, Milpitas, CA, USA) was used to estimate the FDR. Scaffold Q+ (Proteome Software, Portland, OR, USA) was used to compare spectral counts, validate MS/MS-based peptides, identify proteins (FDR < 1% in at least 2 peptides), and calculate Log2-fold changes (FC) and *P* values (Student's *t* test). Differentially expressed proteins (FC > 2, and *P* values < 0.05) were uploaded to the web-based Ingenuity Pathway Analysis (IPA®) software (Version 26127183; QIAGEN) for functional analysis and protein interaction networks.

Statistical analysis

The data are expressed as the mean ± SEM and were analyzed using a two-sided, unpaired Student's *t* test. The mean value between groups was compared using GraphPad Prism 5.0 software (GraphPad Software, La Jolla, CA, USA) unless otherwise indicated. *P* values < 0.05 were considered statistically significant.

Results

GPCR19 colocalizes with P2X7R in microglia

Primary microglia from the brains of C57BL/6 (B6), P2X7R$^{-/-}$, or GPCR19$^{-/-}$ mice were sorted using a magnetic column. The purity was above 95% (Figure 1a). GPCR19 and P2X7R were colocalized in resting primary microglial membranes (Figure 1b) from B6 mice. The expression of P2X7R in P2X7R$^{-/-}$ mice was not apparently like the expression of GPRCR19 in GPCR19$^{-/-}$ mice, which did not confirm the functional knockout of P2X7R$^{-/-}$ or GPCR19$^{-/-}$ mice.

GPCR19 and P2X7R are differentially expressed in the AD brain

The expression levels of GPCR19 in the frontal cortex were significantly lower in 6- and 9-month-old 5xFAD mice than in 3-month-old 5xFAD mice or B6 mice (Figure 3). In comparison, the expression levels of P2X7R in the frontal cortex were significantly higher in 9-month-old 5xFAD mice than in 3-month-old 5xFAD mice or B6 mice (Figure 3). Brain tissues from individuals with AD or without AD were analyzed after immunohistochemical staining. GPCR19 and P2X7R were colocalized in the brain cells of non-AD subjects (Figure 4). The expression of GPCR19 in non-AD subjects (n = 3) was higher than that in AD patients (n = 5). In contrast, the expression of P2X7R in non-AD subjects was lower than that in AD patients.

TDCA inhibit IL-1β and TNF-α expression in microglia

We tested IL-1β secretion by BV2 microglial cells in response to Aβ (2 μM) ± ATP (1 mM) or TDCA (400 ng/ml) to optimize the experimental settings (Figure 2a). IL-1β secretion was increased upon treatment with Aβ alone and was further increased when Aβ was combined with ATP. However, ATP or TDCA alone did not increase IL-1β secretion. Primary microglia from the brains of C57BL/6 (B6),

P2X7R$^{-/-}$, or GPCR19$^{-/-}$ mice were stimulated with Aβ (2 μM) and ATP (1 mM). The IC_{50} of TDCA in inhibiting IL-1β secretion by microglia from B6 mice was 490.6 nM (Figure 2b). However, TDCA did not inhibit IL-1β secretion by microglia from GPCR19$^{-/-}$ or P2X7R$^{-/-}$ mice when stimulated with Aβ (2 μM) and ATP (1 mM) (Figure 2b), suggesting that GPCR19 might control P2X7R function. TDCA was compared with semisynthetic GPCR19 agonist (INT777), P2X7R antagonist (A 740003, GW791343) and NLRP3 inhibitor (MCC950) in terms of inhibiting pro-inflammatory cytokine IL-1β and TNF-α. TDCA significantly inhibited IL-1β and TNF-α in microglia cell stimulated by Aβ ± ATP/BzATP. The EC_{50} of TDCA is 0.45uM shows potent anti-inflammatory function more specifically suppressing both IL-1β and TNF-α is considered for the treatment of choice against chronic inflammatory disease like AD.

TDCA regulates the expression of GPCR19 and P2X7R in microglia.

Treatment of BV2 cells with Aβ ± ATP for 1 h significantly downregulated the expression of GPCR19 on the cell surface, while this effect was reversed by TDCA treatment (Figure 5a). In contrast, the surface expression of P2X7R was upregulated by Aβ ± ATP and was inhibited by TDCA treatment (Figure 5a). In BV2 cells, GPCR19 (green) and P2X7R (red) showed colocalization (yellow) in the resting state (Figure 5a). The colocalized area decreased after treatment with Aβ ± ATP, which was upregulated by TDCA treatment (Figure 5b).

In the frontal cortex of 5xFAD mice, GPCR19 expression was significantly increased after treatment with TDCA (1 mg/kg, i.p., q.d. for 10 weeks) compared with PBS-treated mice (Figure 6a). However, the expression levels of P2X7R were significantly lower in 5xFAD-TDCA mice than in 5xFAD-PBS mice (Figure 6a). Colocalization areas (yellow) of GPCR19 (green) with P2X7R (red) in the brain

were significantly lower in 5xFAD-PBS mice than in 5xFAD-TDCA mice (Figure 6b).

Roles of GPCR19 in P2X7R-mediated Ca^{++} mobilization in microglia.

Primary microglia were isolated from the brains of B6, $P2X7R^{-/-}$, or $GPCR19^{-/-}$ mice. In response to P2X7R agonists (ATP or BzATP), Ca^{++} mobilization was significantly decreased in microglia from $P2X7R^{-/-}$ or $GPCR19^{-/-}$ mice compared with microglia from B6 mice (Figure 7a, b). When treated with Aβ, Ca^{++} mobilization of BV2 cells was significantly inhibited by TDCA in response to BzATP in a dose-dependent manner (Figure 8). ATP (Figure 9a) or BzATP (Figure 9b) increased Ca^{++} mobilization of BV2 microglial cells in the presence of Aβ, and Ca^{++} mobilization was significantly inhibited by TDCA (400 ng/ml).

TDCA suppresses N3I activation of microglia via Aβ ± ATP.

When BV2 cells were treated with Aβ (2 μM) ± ATP (1 mM), the transcript levels of NLRP3, ASC, pro-caspase-1, and proIL-1β were increased (Figure 10). Although Aβ (2 μM) alone increased these transcripts, ATP alone did not increase these transcript levels (but proIL-1β), suggesting that Aβ (2 μM) alone could activate the priming phase of the NLRP3 inflammasome. TDCA significantly inhibited the upregulation of these transcripts increased by Aβ ± ATP. In primary microglial cells, Aβ treatment significantly increased the expression of NLRP3 and ASC (Figure 11). Treatment with Aβ + ATP further increased the expression of NLRP3. Aβ ± ATP treatment increased the expression of NLRP3 and ASC in the nucleus (white arrows) and in the cytosolic compartment (yellow, Figure 11a). TDCA treatment significantly suppressed the expression of these two molecules, as well as their colocalization (yellow dots, Figure 3b). Interestingly, the levels of nuclear NLRP3 (white arrows) were significantly downregulated by TDCA treatment. Caspase-1 secretion from primary microglia treated with Aβ + ATP was inhibited by TDCA treatment (Figure 3c).

In BV2 cells, treatment with Aβ + ATP increased the expression of NLRP3. Aβ ± ATP treatment increased the expression of NLRP3 and ASC in the nucleus (white) and in the cytosolic compartment (yellow, Figure 12a). TDCA treatment significantly suppressed the expression of these two molecules as well as their colocalization (yellow dots, Figure 12b. *In vivo,* TDCA administration (1 mg/kg, i.p., q.d.) for 10 weeks decreased the expression of NLRP3 and ASC in the frontal cortex of 5xFAD mice compared with PBS-treated 5xFAD mice (Figure 13).

TDCA inhibited proinflammatory cytokine and ROS production in microglia via Aβ ± ATP.

To elucidate how TDCA inhibits the transcription and expression of N3I components, we analyzed the GPCR19-cAMP-PKA-NF-kB axis after BV2 cells were treated with Aβ ± TDCA (Figures 14 and 15). TDCA increased cAMP production in BV2 cells irrespective of Aβ treatment (Figure 15). Adenylyl cyclase inhibitor (KH7) blocked TDCA-mediated cAMP production in BV2 cells. BV2 cells increased the production and secretion of IL-1β, IL-18, and TNF-α upon treatment with Aβ ± ATP, while TDCA suppressed the production of these cytokines (Figure 14). BV2 cells produced ROS in response to Aβ, and ROS production was inhibited by TDCA treatment (Figure 15).

TDCA decreases apoptosis of neurons in 5xFAD mouse brains.

$NeuN^+$ cells in the brains of 5xFAD mice were stained after treatment with TDCA for 10 weeks (1 mg/kg, i.p., q.d., Figures 16 and 17). The cortexes (Figure 16) and hippocampi (CA1, CA3, and DG) (Figure 17) were observed using confocal microscopy. The number of $NeuN^+$ cells in the cortex was significantly higher in 5xFAD mice treated with TDCA than in 5xFAD mice treated with PBS (Figure 16 a and b). The mean fluorescent intensity (MFI) of the $NeuN^+$ area in the hippocampi of 5xFAD mice was significantly higher in the TDCA group than in the PBS group

(Figure 17). The MFI of TUNEL+ apoptotic cells in the cortex was significantly higher in 5xFAD mice treated with PBS than in 5xFAD mice treated with TDCA (Figure 16).

TDCA decreases gliosis and Aβ plaques in the brains of 5xFAD mice.

After i.p. administration of TDCA for 10 weeks, the numbers of Iba-1^{+} reactive microglia in the cortex and dentate gyrus (DG) (Figure 18) of the hippocampus decreased. The number of GFAP^{+} reactive astrocytes also significantly decreased in the cortex (Figure 19a), DG (Figure 19b), and CA3 regions (Figure 19c) of the hippocampus in 5xFAD mice upon treatment with TDCA. The numbers of Aβ plaques and the total area of plaques (white arrows) in the cortex and hippocampus of 5xFAD mice decreased after TDCA treatment (Figure 20).

TDCA increases the expression of scavenger receptor (SR) A and phagocytosis of Aβ

We further investigated the effects of TDCA on SRA, since the expression of SRA was increased by TDCA treatment in the proteomic analysis of 5xFAD mouse brains. *In vitro*, treatment of BV2 cells with Aβ significantly downregulated SRA expression, which was normalized by TDCA (Figure 21a). SRA transcripts were significantly downregulated in BV2 cells upon treatment with Aβ for 24 h and were dose-dependently increased by TDCA treatment (Figure 21b). *In vivo*, CD11b^{int}CD45^{int} primary microglia isolated from the brains of 5xFAD mice treated with TDCA for 10 weeks showed significantly higher SRA levels than microglia from PBS-treated 5xFAD mice (Figure 21c). Since P2X7 is known to inhibit phagocytosis and SRA is known to increase phagocytosis, we hypothesized that TDCA-induced suppression of P2X7 expression and TDCA-induced SRA expression might contribute to increased phagocytosis of Aβ by microglia. As expected, primary microglia from B6 mice showed decreased expression of P2X7R and increased

phagocytosis of fluorescent Aβ oligomers (fAβ) upon treatment with TDCA (Figure 22a). Interestingly, P2X7R^{high} microglia (white arrows) did not phagocytose fAβ even after treatment with TDCA (Figure 22a). After being phagocytosed, fAβ was colocalized with LAMP-2^{+} phagosomes in BV2 cells, and the process was enhanced by TDCA treatment (Figure 22b).

Proteogenomic analysis of brain tissues of 5xFAD mice treated with TDCA.

After administration of TDCA (1 mg/kg, i.p., q.d.) for 10 weeks, the proteomes of brain tissues from 5xFAD mice were analyzed (Figure 23a, b). A total of 3,259 unique proteins were identified at a protein threshold of a 1.0% false discovery rate (FDR). Among these proteins, 460 proteins showing peptide spectral counts in more than two assays from triplicate assays, with a fold change of more than 2 between PBS- and TDCA-treated groups, are depicted on the heatmap, plotted with the Perseus software platform (http://www.perseus-framework.org). Proteomic analysis indicated that 56 proteins exhibited more than 2-fold changes in the 95% confidence interval (Figure 23a), demonstrating two distinct proteome clusters that were upregulated in TDCA-treated groups and downregulated in PBS-treated groups, or vice versa. The functions of these proteins were further analyzed based on QIAGEN's IPA database (Figure 23b). Notably, a canonical pathway, regulation of eIF4 and p70S6K, was enriched by TDCA treatment, suggesting that TDCA plays critical roles in translational regulation followed by calcium signaling, which could exert allosteric regulatory effects on many enzymes and proteins. Based on proteomic analysis, we further analyzed the transcript levels of several proinflammatory cytokines in both the hippocampi and cortices of 5xFAD mice after TDCA treatment for 10 weeks. TDCA downregulated IL-1β, TNF-α, IL-33, IL-12, CCL-11, and CCL-5 transcripts. In contrast, TDCA treatment increased the transcript levels of IFN-γ, IL-10, CCL-17, and GPCR19, CD47, FPR-2, CD36, SRB1, and SRA in the brains of 5xFAD mice (Figure 24).

TDCA improves the spatial learning and memory of 5xFAD mice.

B6 and 5xFAD mice were administered PBS or TDCA for 10 weeks (1 mg/kg, i.p., q.d.), and spatial learning and memory were assessed using the Morris water maze (MWM) test (Figure 25a). There were no significant changes in body weight after TDCA treatment for 10 weeks (Figure 25b). Escape latency decreased over the 4-day training period in all three groups. Mice in the TDCA group showed a significant reduction in time latency to reach the platform (Figure 26a), which was comparable to that of B6 mice. In the probe test on day 5, TDCA-treated 5xFAD mice showed increased numbers of platform crossings (Figure 26b). TDCA-treated 5xFAD mice remained for longer periods of time in the target quadrant than in the opposite quadrant compared with PBS-treated 5xFAD mice (Figure 26c). Times in the target quadrant and on the platform of the 5xFAD-TDCA group were comparable to those of B6 mice. TDCA-treated 5xFAD mice spent more time on the platform than the PBS group (26 d). The movement of 5xFAD mice treated with PBS was relatively random and disorganized compared with that of B6 mice and TDCA-treated 5xFAD mice (Figure 26e).

Spatial learning and memory were also assessed using a Y-maze test and novel object recognition test (NOR). In the Y-maze test, the alternation percentage of the mice in the 5xFAD-PBS group was significantly lower than that of mice in the B6-PBS group and 5xFAD-TDCA group (Figure 27a). In the NOR test, exploration time to a new object compared to an old object was significantly higher in B6-PBS and 5xFAD-TDCA mice (Figure 27b). 5xFAD-PBS mice did not exhibit a difference in exploration time between old and new objects. The discrimination index for the mice in the 5xFAD-TDCA group was significantly higher than that for mice in the 5xFAD-PBS group (Figure 27c).

Oral administration of TDCA shows efficacy in 5xFAD mice.

B6 mice were administered PBS, TDCA or TDCA formulated with carboxymethyl cellulose CMC (0.5%). The PK profile of plasma and brain TDCA concentration were depicted for 48h (Figure 28). The $AUC_{(last)}$ of TDCA in plasma and brain is 3341.98 ng/ml and 2657.64 ng/ml respectively (Table 3). After oral administration of formulated TDCA (30 mg/kg, p.o., b.i.d.) for 14 weeks, spatial learning and memory of mice were also tested. No obvious changes in body weight were observed (Figure 29). The escape latency of mice in the 5xFAD-TDCA group decreased (Figure 30a). In the probe test on day 5, 5xFAD-TDCA mice exhibited increased numbers of crossings over the target quadrant (Figure 30bi). 5xFAD-TDCA mice remained in the target quadrant for longer periods of time and spent less time in the opposite quadrant than 5xFAD-vehicle mice (Figure 30c). Spatial learning and memory were also assessed by the NOR test after feeding TDCA orally (Figure 30d). The discrimination index (%) of the mice in the 5xFAD-vehicle group was significantly lower than that of mice in the 5xFAD-TDCA group (Figure 30d). 5xFAD-TDCA mice exhibited decreased Aβ plaques in the cortex and hippocampus (Figure 31a). Cellular apoptosis also decreased in the 5xFAD-TDCA mouse brain, as shown by the increased number of $NeuN^+$ cells after TDCA administration (Figure 31b).

Figures

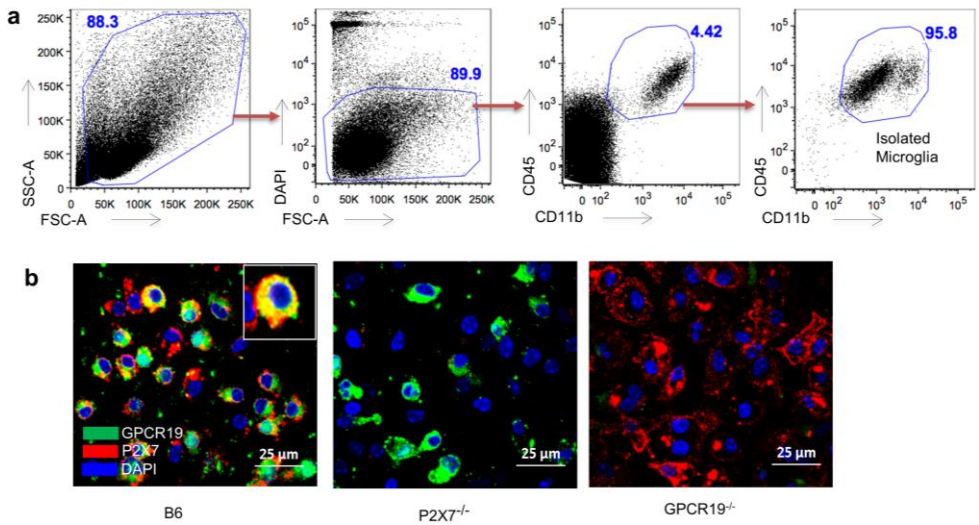

Figure 1. GPCR19 and P2X7R are colocalized in microglia

a, Representative gating strategies of flow cytometry to determine the purity of isolated primary microglia. $DAPI^-$ $CD11b^+CD45^+$ cells were gated. **b,** Primary microglia isolated from B6, $GPCR19^{-/-}$, and $P2X7R^{-/-}$ mice were immune-stained. The expression levels of GPCR19 or P2X7R were determined by measuring the MFI of ROIs in individual channels after staining with anti-GPCR19 antibody (green) and anti-P2X7R antibody (red). The nuclei were stained with DAPI (blue). Merged (GPCR19 (green) + P2X7R (red)) channels show the colocalization area (yellow).

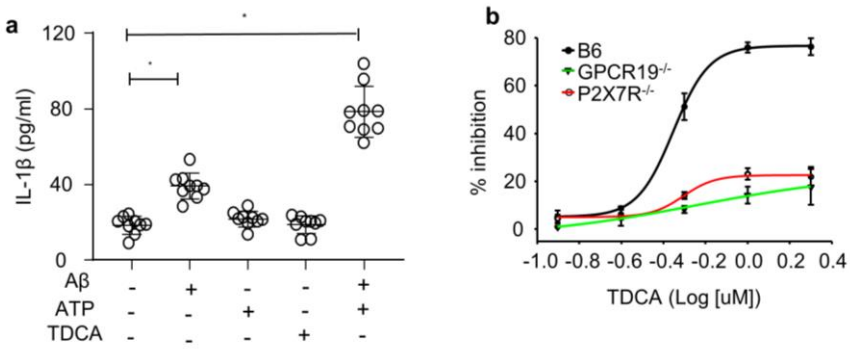

c

Agent	Mode of Action	Aβ		Aβ+ ATP		Aβ+ BzATP	
		IL-1β	TNF-α	IL-1β	TNF-α	IL-1β	TNF-α
TDCA	**GPCR19 agonist**	25	46	75	48	72	42
INT777	GPCR19 agonist	15	17	20	32	26	23
MCC950	NLRP3 inhibitor	11	4	92	18	85	8
A 740003	P2X7 receptor antagonist	17	9	9	21	83	11
GW791343	Allosteric inhibitor of P2X7 receptor	23	12	8	29	71	28

% of inhibition

100 90 80 70 60 50 40 30 20 10 0

Figure 2. TDCA suppressed Aβ ± ATP/BzATP induced IL-1β and TNF-α in microglia

a, Aβ ± ATP increased IL-1β production in BV2 cells, as measured by ELISA. **b,** Primary microglia isolated from wild-type B6, P2X7R$^{-/-}$, and GPCR19$^{-/-}$ mice and treated with Aβ, ATP, and TDCA. Aβ, ATP and TDCA were used at concentrations of 2 μM, 1 mM and 400 ng/ml, respectively, throughout the study unless otherwise indicated. IL-1β production by microglia was determined by ELISA. BV2 cells were treated with Aβ ± ATP/BzATP for 24h with or without TDCA, INT777, MCC950, A

740003 and GW791343. 500uM BzATP and 1uM of TDCA, INT777, MCC950, A 740003 and GW791343 were used. IL-1β or TNF-α production by microglia was determined by ELISA. % Inhibition = (IL-1β/TNF-α concentration without TDCA - IL-1β/TNF-α concentration with TDCA) / (IL-1β/TNF-α concentration without TDCA) x 100. Data are from more than three independent experiments throughout the study otherwise denoted. The individual samples are shown with the mean ± SEM and *P < 0.05 using Student's unpaired t test throughout the study otherwise denoted.

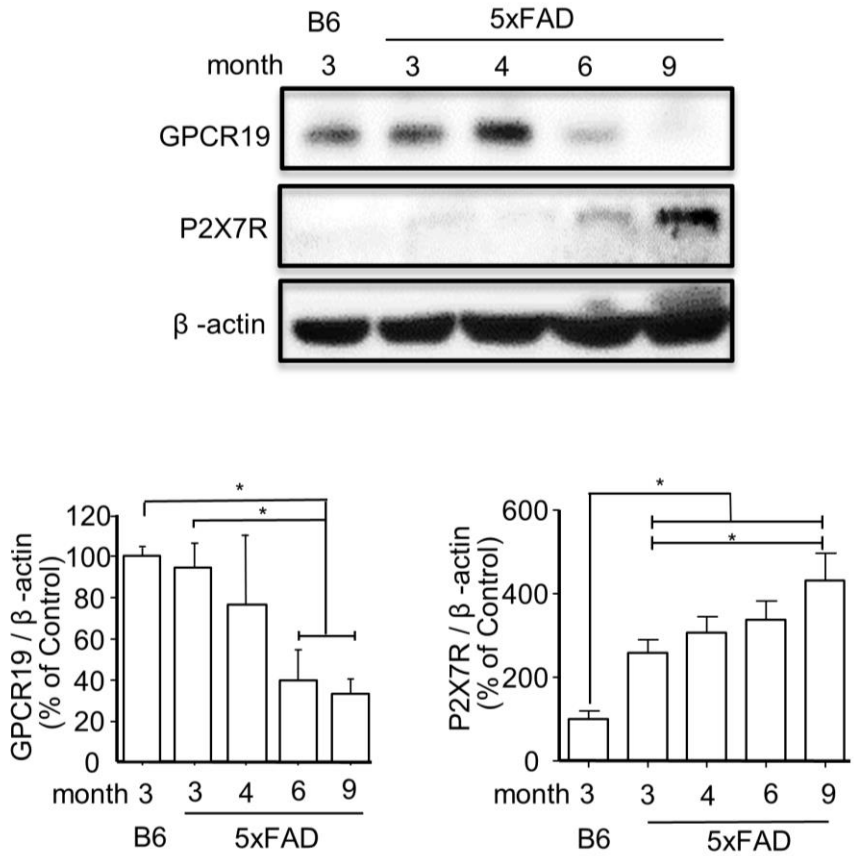

Figure 3. The expression of GPCR19 and P2X7R in 5xFAD mice changes with age.

Protein expression levels of GPCR19 or P2X7R in the frontal cortex of B6 (3 months old) and 5xFAD (3, 4, 6 and 9 months old) mice were analyzed using western blotting. The expression levels in B6 mice were considered 100% (n=3).

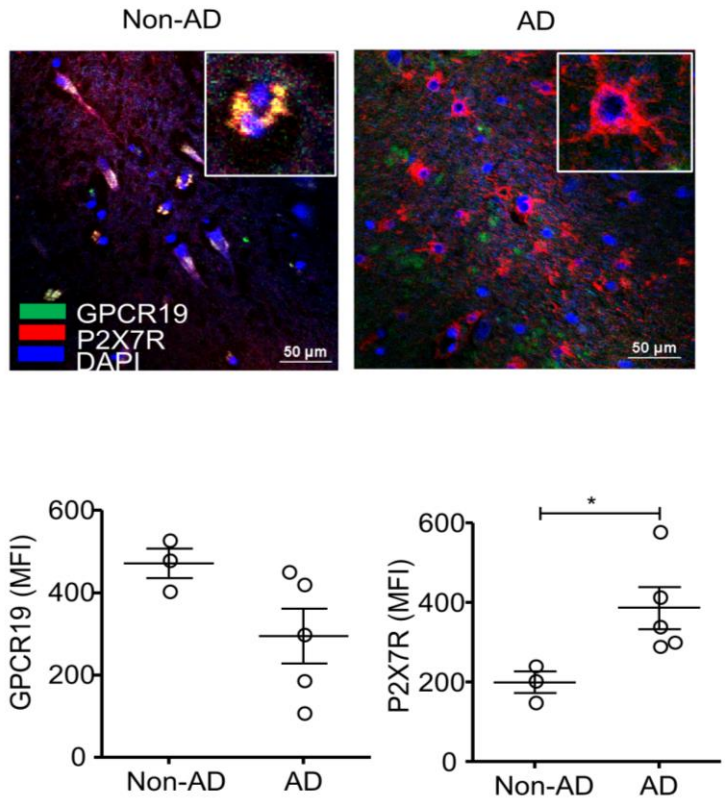

Figure 4. The brains of AD patients express higher levels of P2X7R than those of non-AD patients.

Human brain sections from patients with AD or patients without AD (non-AD, n=3) were stained with anti-GPCR19 Ab (green) and anti-P2X7R Ab (Red). The nuclei were stained with DAPI (blue). Merged (GPCR19 (green) + P2X7R (red)) channels show the colocalization area (yellow).

The average of five different ROIs (× 400) in each section was analyzed and is shown in the right panel.

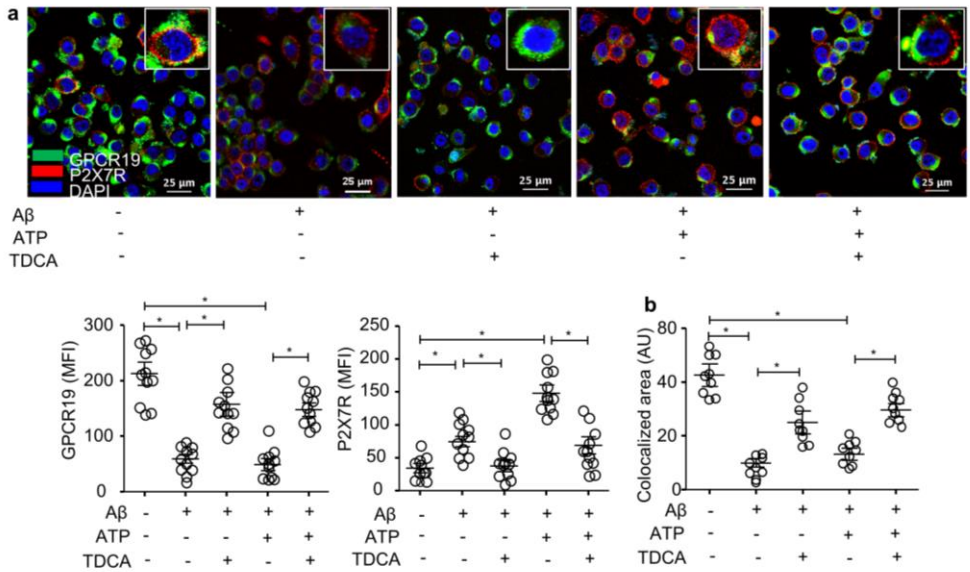

Figure 5. TDCA induces GPCR19R, suppresses P2X7R and increases its colocalization.

a, The expression levels of GPCR19 (green) and P2X7R (red) on the surface of BV2 cells were analyzed using confocal microscopy after treatment with Aβ (2 μM), TDCA (400 ng/ml), and ATP (1 mM) for 1 h. The nuclei were stained with DAPI (blue). **b,** The areas of colocalization (yellow) of GPCR19 (green) and P2X7R (red) were calculated using ImageJ.

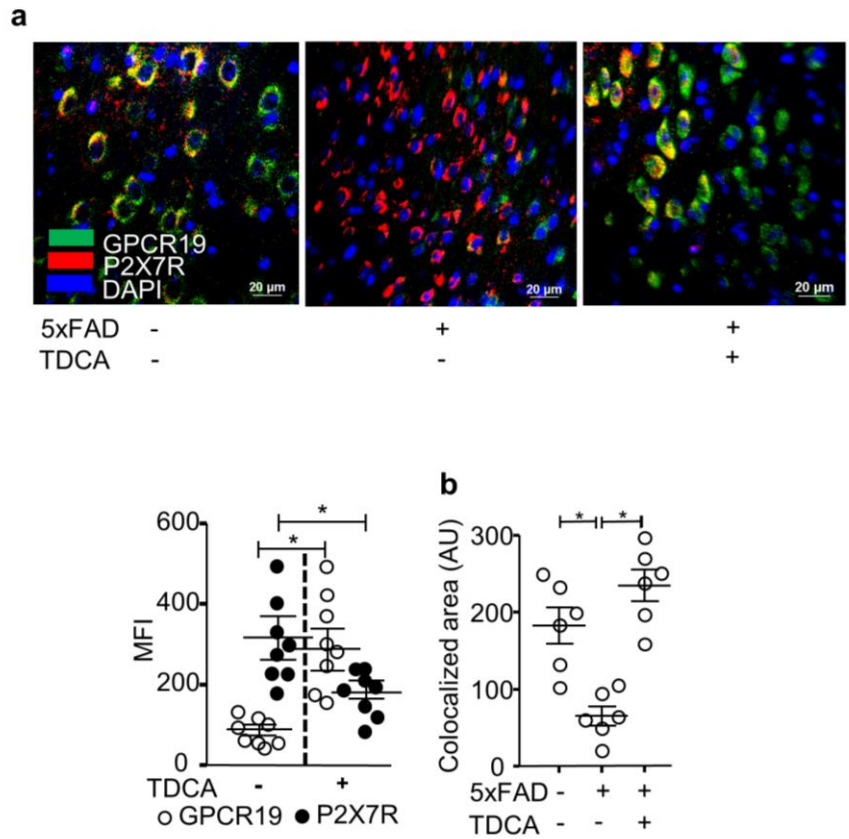

Figure 6. TDCA induces GPCR19R, suppresses P2X7R and increases its colocalization in 5xFAD mouse brains.

a, The frontal cortex of 5xFAD mice treated with TDCA (1 mg/kg, i.p., q.d.) for 10 weeks (n = 6/group) were analyzed using confocal microscopy after staining for GPCR19 (green) and P2X7R (red). The nuclei were stained with DAPI (blue). **b,** Colocalized areas of GPCR19 and P2X7R (yellow) were calculated using ImageJ.

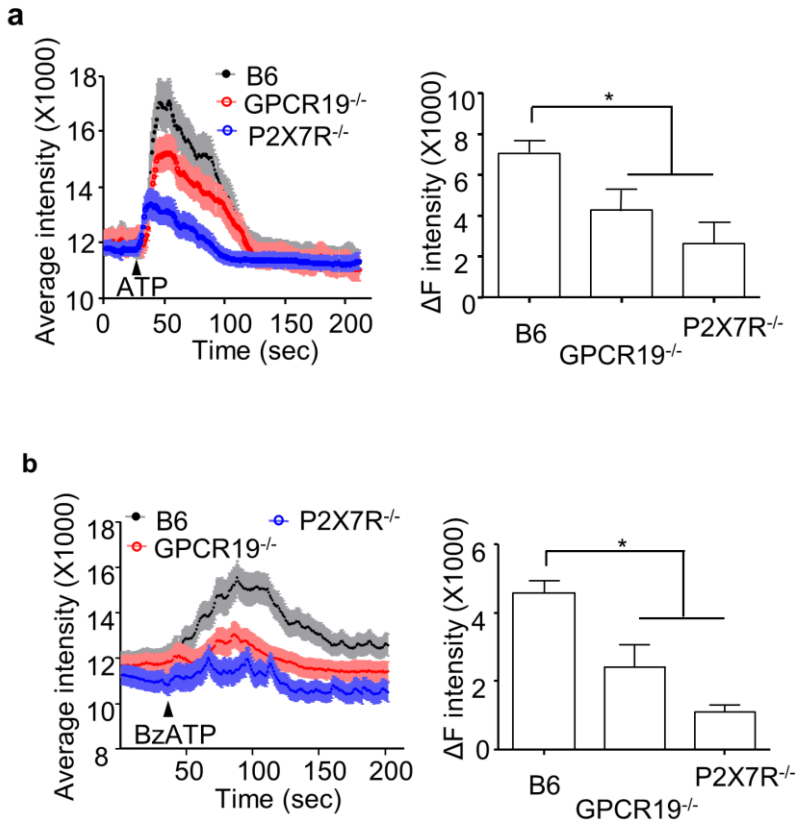

Figure 7. Decreased Ca^{++} mobilization in primary microglia of P2X7R$^{-/-}$ and GPCR19$^{-/-}$ mice

a, b, Primary microglia from B6, GPCR19$^{-/-}$, and P2X7R$^{-/-}$ mice (n = 6/group) were stimulated with ATP (**a**) (40 μM) or BzATP (**b**) (40 μM). Average intensity reflecting intracellular Ca^{++} mobilization (shown in the left panels) and delta intensity (max-min) after stimulation were analyzed (right panel).

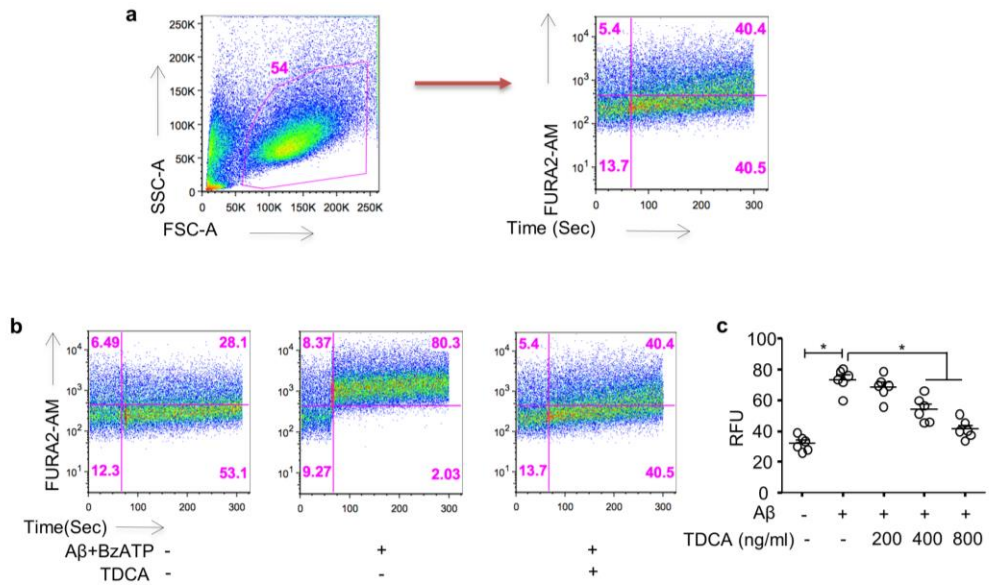

Figure 8. TDCA inhibited Ca^{++} mobilization in BV2 cells induced by Aβ + BzATP

a, A gating strategy of flow cytometry to determine intracellular Ca^{++} in BV2 cells after staining with FURA2-AM. The amount of Ca^{++} in cells was analyzed by using Ca^{++} binding dye (FURA2-AM) for 300 sec. BzATP was added at 60 sec. **b,** Ca^{++} mobilization of BV2 cells was measured after treatment with Aβ, BzATP (300 μM), and TDCA using flow cytometry. Representative FACS plots are shown in the left panels, and **c,** RFUs from three independent experiments are depicted in the right panel.

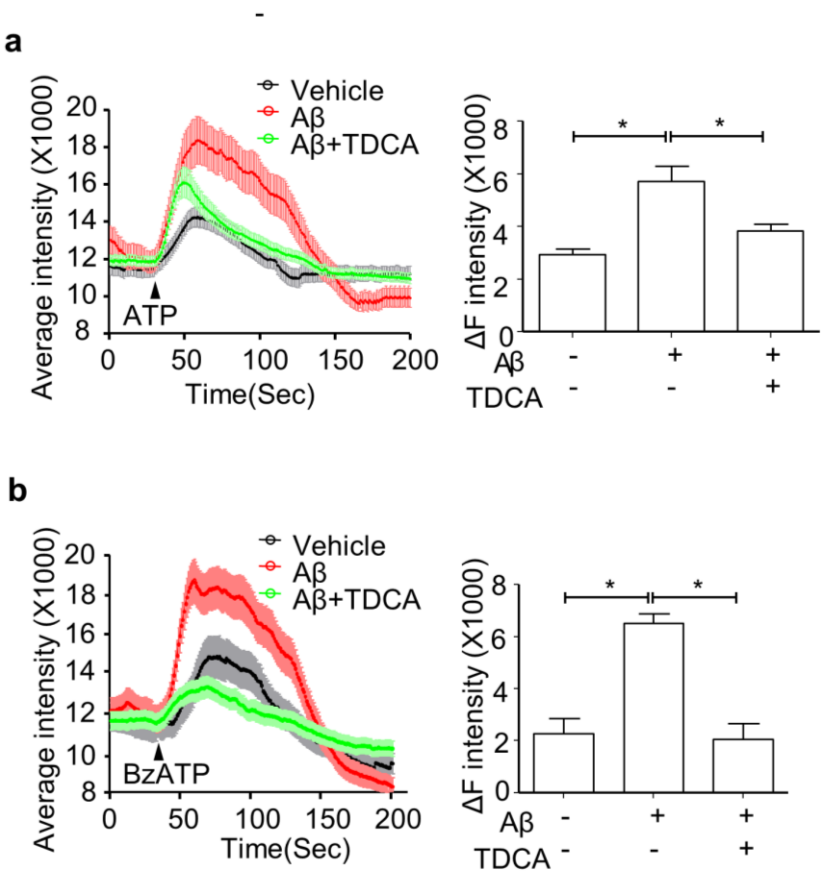

Figure 9. TDCA inhibited Ca^{++} mobilization in BV2 cells induced by Aβ + ATP/BzATP

Ca^{++} mobilization of BV2 cells in response to Aβ and TDCA in the presence of ATP (**a**) (40 μM) or BzATP (**b**) (40 μM). Average intensity reflecting intracellular Ca^{++} mobilization (shown in the left panels) and delta intensity (max-min) after stimulation were analyzed (right panel).

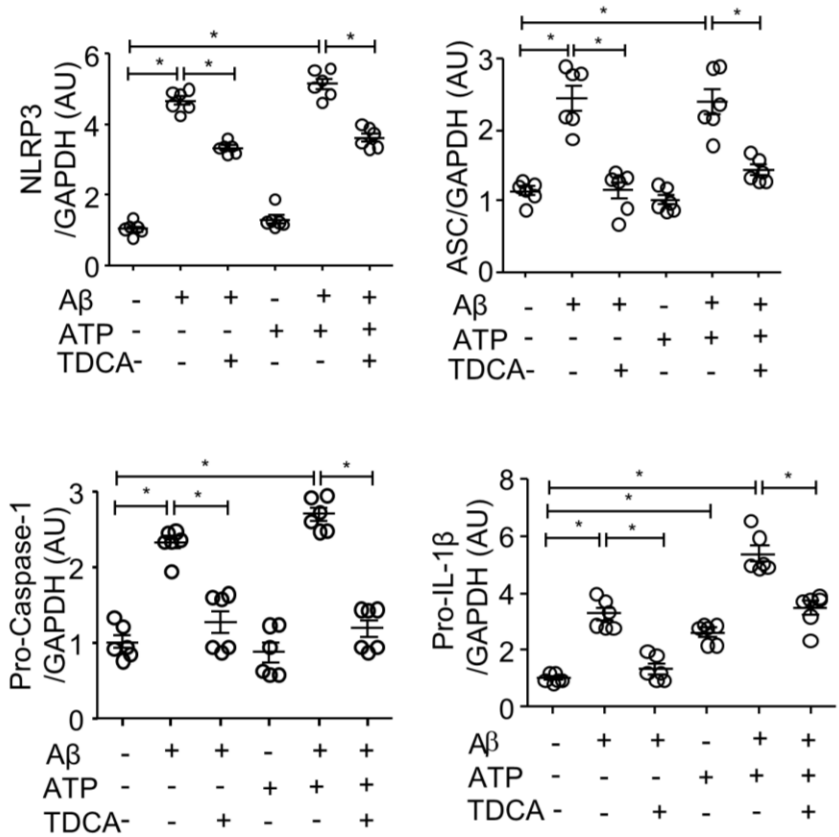

Figure 10. TDCA suppresses activation of the NLRP3 inflammasome in BV2 cells

Transcripts of *NLRP3, ASC, pro-caspase-1,* and *IL-1β* in BV2 cells were quantitated using qPCR after treatment with Aβ, TDCA, and ATP. Aβ (2 μM) and TDCA (400 ng/ml) were added for 24 h, and ATP (1 mM) was added for 1 h. Gene expression was normalized using *GAPDH.*

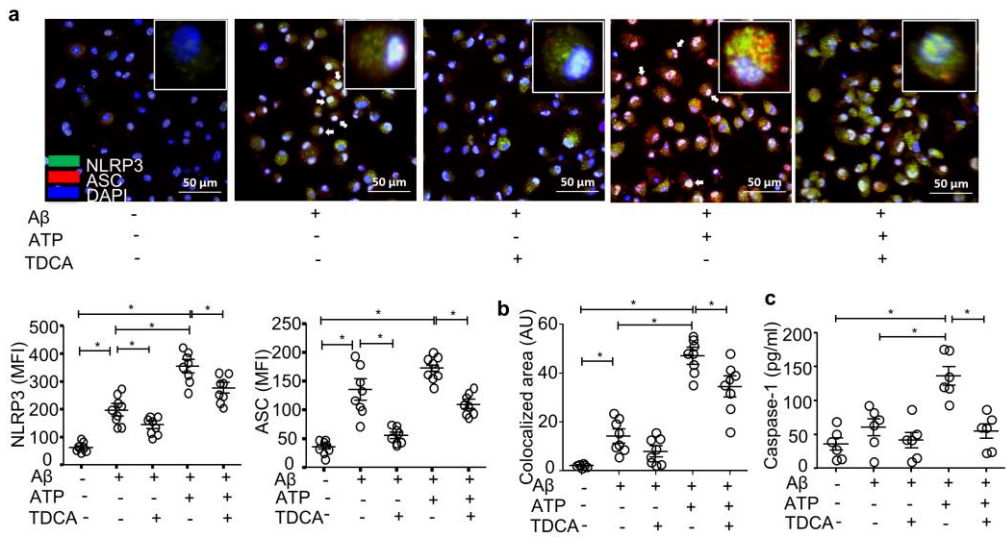

Figure 11. TDCA suppresses NLRP3 inflammasome complex formation in primary microglia.

a, The expression of NLRP3 (green) and ASC (red) in primary microglia was determined using confocal microscopy. Nuclei were stained with DAPI (blue). **b,** Colocalization of NLRP3 and ASC (yellow) was analyzed using ImageJ. **c,** Concentrations of caspase-1 in culture supernatants of primary microglial cells were analyzed using ELISA.

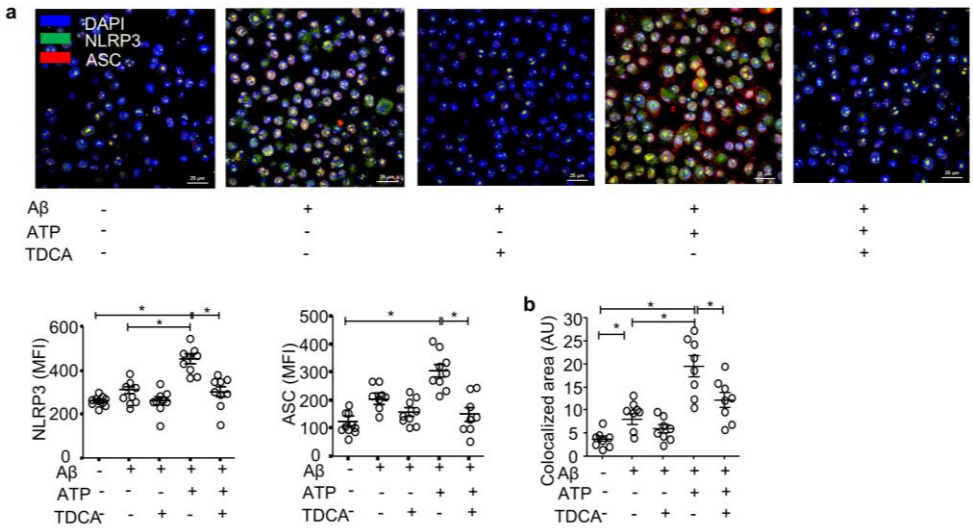

Figure 12. TDCA suppresses NLRP3 inflammasome complex formation in BV2 cells.

a, The expression of NLRP3 (green) and ASC (red) in BV2 cells was determined using confocal microscopy. Nuclei were stained with DAPI (blue). **b,** Colocalization of NLRP3 and ASC (yellow) was analyzed using ImageJ.

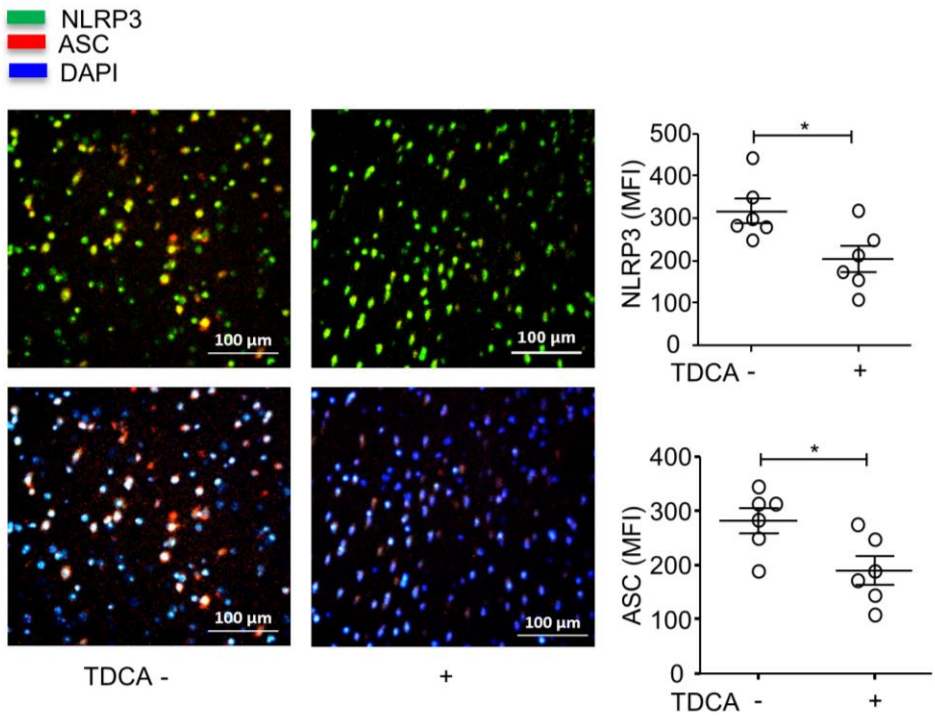

Figure 13. TDCA suppresses the expression of NLRP3 inflammasome complex protein in 5xFAD mouse brains.

5xFAD mice (n = 6/group) were treated with 1 mg/kg TDCA i.p. for 10 weeks, and the expression levels of NLRP3 (green) and ASC (red) in the frontal cortex were analyzed using confocal microscopy. The nuclei were stained with DAPI (blue). Merged (NLRP3 (green) + ASC (red)) channels show yellow colocalization areas and merged (NLRP3 (green) + ASC (red) + nuclei (blue)) channels show white colocalization areas.

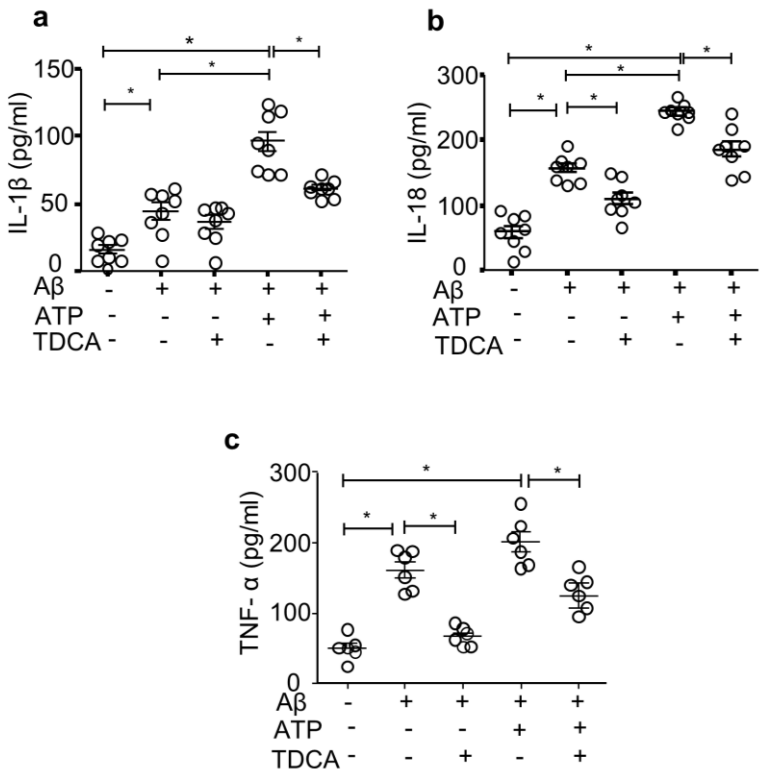

Figure 14. TDCA suppresses the production of IL-1β, IL-18 and TNF-α in BV2 cells

BV2 cells were also cultured in the presence Aβ, TDCA, and ATP. Aβ (2 μM) and TDCA (400 ng/ml) were added for 24 h, and ATP (1 mM) was added for 1 h. IL-1β (**a**), IL-18 (**b**), and TNF-α (**c**) in the culture supernatants of BV2 cells were analyzed using ELISA.

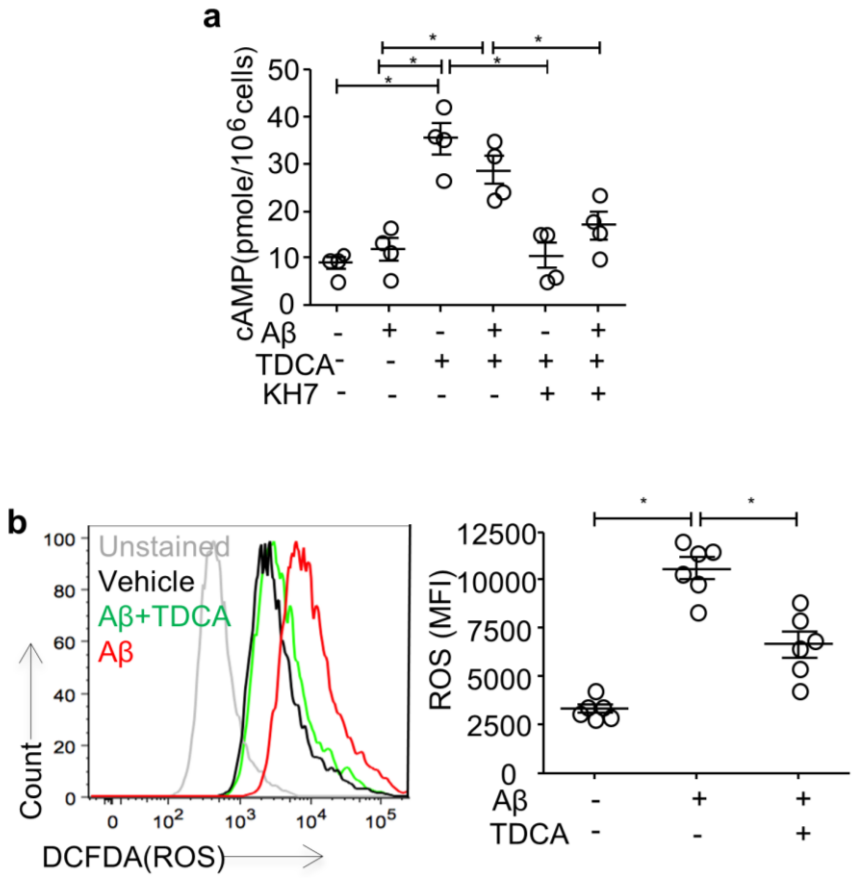

Figure 15. TDCA induces cAMP production and suppresses ROS in microglia. **a,** The level of cAMP in the BV2 cell lysates was measured. BV2 cells were also cultured in the presence of the adenylate cyclase inhibitor KH7 (4 μM). The culture supernatants of BV2 cells were analyzed using ELISA. **b,** ROS production in BV2 cells was quantitated using FACS after pulsing cells with DCFDA. A representative FACS plot (left panel) of three independent experiments (right panel) is depicted.

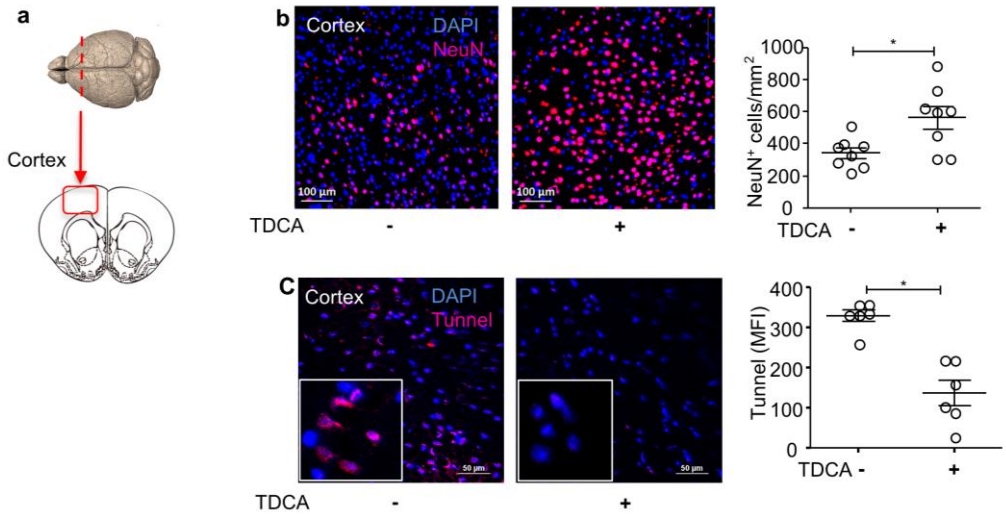

Figure 16. TDCA prevents apoptosis of neurons in the 5xFAD mouse brain cortex.

a, 5xFAD mice (n = 8/group) were treated with 1 mg/kg TDCA i.p. for 10 weeks. $NeuN^+$ cells in the cortex were analyzed using confocal microscopy. **b,** A set of representative images is depicted in the left panel, and the number of $NeuN^+$ cells is shown in the right panel. **c,** Apoptotic cells in the brain were quantitated after TUNEL staining. The nuclei were stained with DAPI (blue).

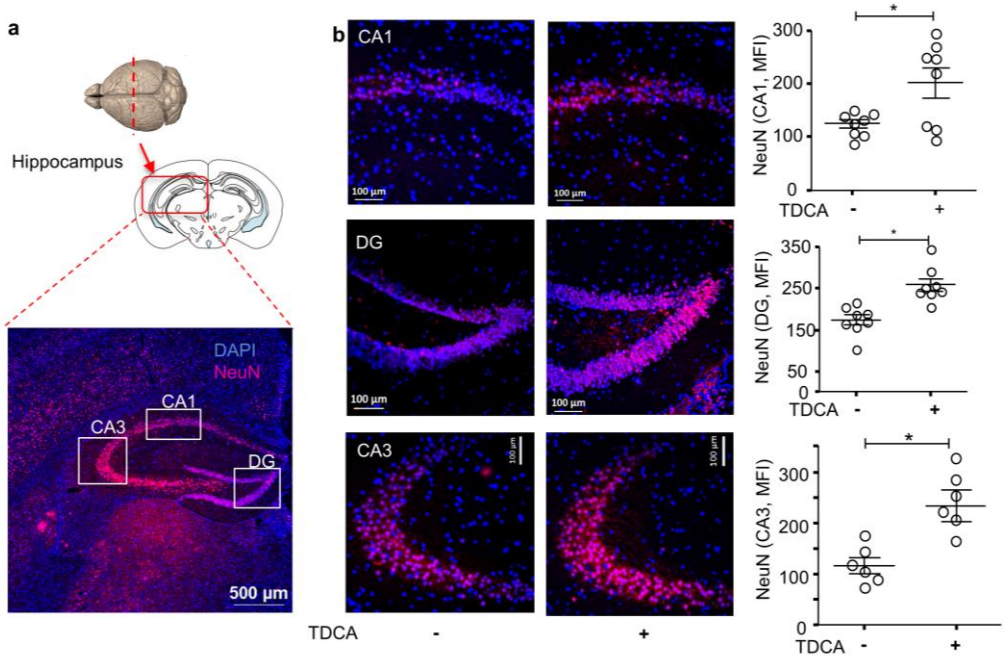

Figure 17. TDCA prevents apoptosis of neurons in the 5xFAD mouse brain hippocampus.

a, 5xFAD mice (n = 8/group) were treated with 1 mg/kg TDCA i.p. for 10 weeks. $NeuN^+$ cells in the hippocampus (CA1, DG and CA3 regions) were analyzed using confocal microscopy. The nuclei were stained with DAPI (blue). A set of representative images is depicted in the left panel, and the MFI ± SEM is shown in the right panel. The MFI ± SEM of specific ROIs (× 400) from the left panel were analyzed in the right panel.

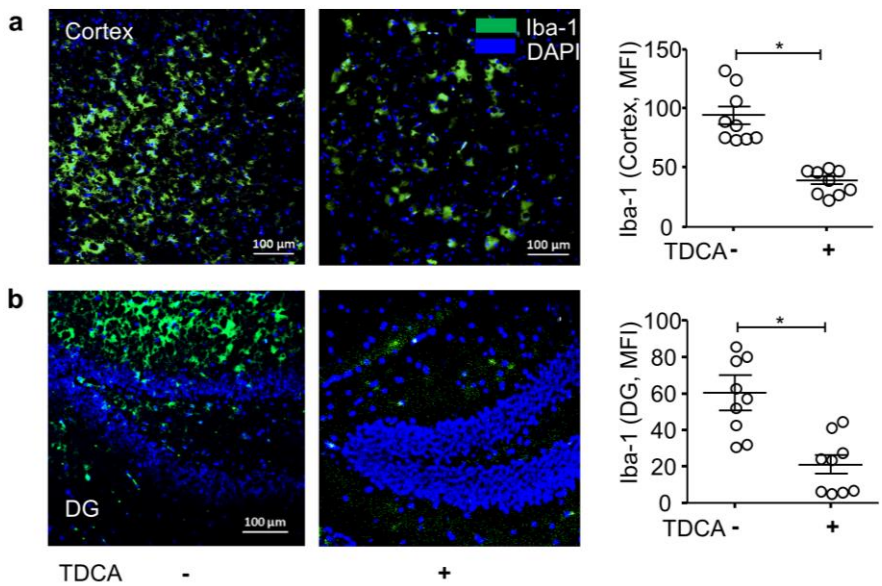

Figure 18. TDCA decreases reactive microgliosis in the brains of 5xFAD mice. Reactive microgliosis in the frontal cortex and DG of 5xFAD mice analyzed with confocal microscopy after staining with anti-Iba-1 Ab (left panel) of 5xFAD mice treated with TDCA (1 mg/kg, i.p., q.d.) for 10 weeks. The nuclei were stained with DAPI (blue).

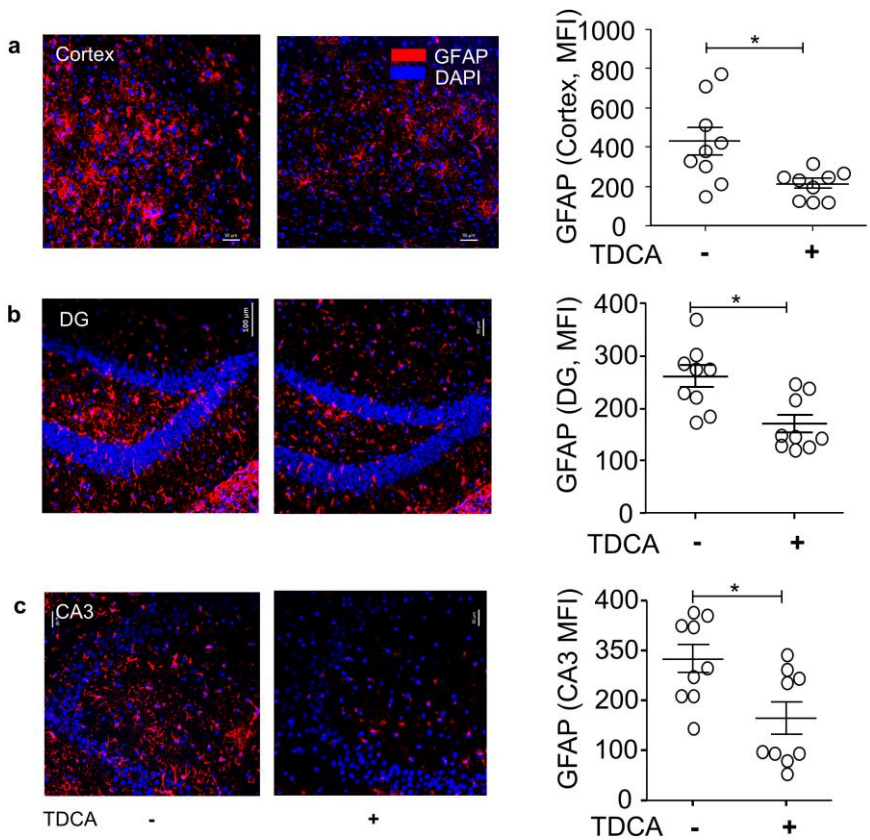

Figure 19. TDCA decreases reactive astrocytes in the brains of 5xFAD mice.

Confocal microscopy showing GFAP$^+$ (red) reactive astrocytes in the cortex (**a**), DG (**b**), and CA3 (**c**) of 5xFAD mice treated with TDCA (1 mg/kg, i.p., q.d.) for 10 weeks. The MFI ± SEM of specific ROIs (× 400) from the left panels (**a, b,** and **c)** were analyzed in the right panel (n = 9 mice/group). The nuclei were stained with DAPI (blue).

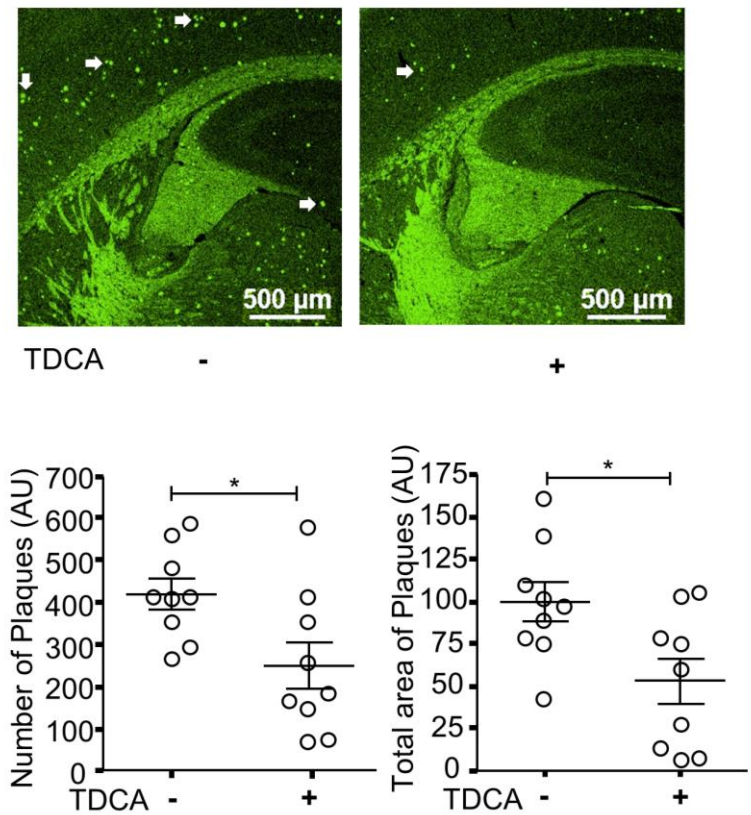

Figure 20. TDCA decreases Aβ plaques in the brains of 5xFAD mice.

Aβ plaques in the brain sections of 5xFAD mice treated with TDCA (1 mg/kg, i.p., q.d.) for 10 weeks were stained with thioflavin-S (green dots indicated with white arrows). The number of plaques and total area of plaques were quantitated using ImageJ.

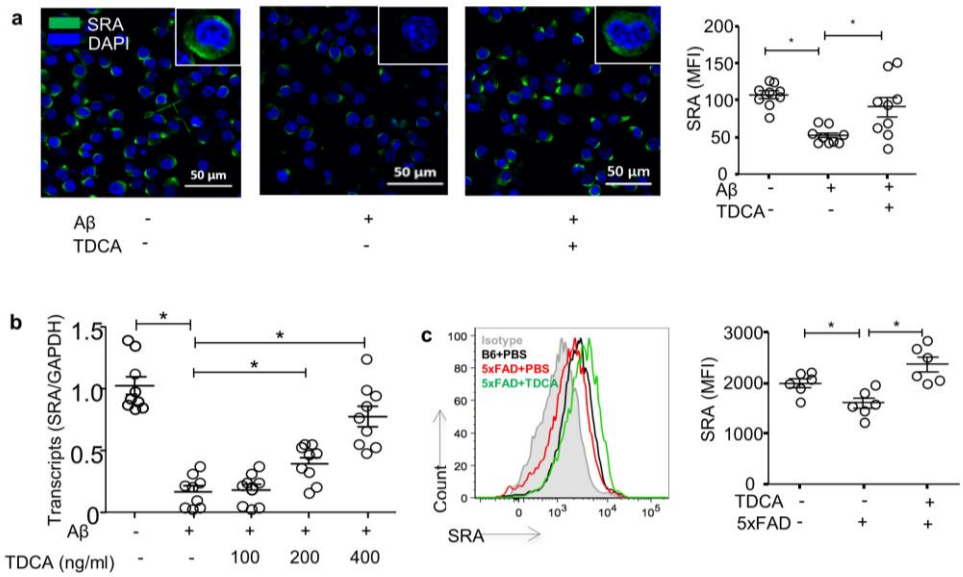

Figure 21. TDCA increases the expression of microglial SRA.

BV2 cells were treated with Aβ (2 µM) ± TDCA (400 ng/ml) for 24 h. **a,** Confocal microscopy of cell surface SRA (green) expression. The nuclei were stained with DAPI (blue). **b,** BV2 cells were treated with different concentrations of TDCA ± Aβ (2 µM) for 24 h. *SRA* transcript levels were determined using qPCR and were normalized to *GAPDH* transcript levels. **c,** Surface expression of SRA on $CD11b^{int}CD45^{int}$ microglial cells from 5xFAD or B6 mice was determined using flow cytometry. A representative FACS plot (left panel) and MFI ± SEM of n = 6 mice/group (right panel) were analyzed.

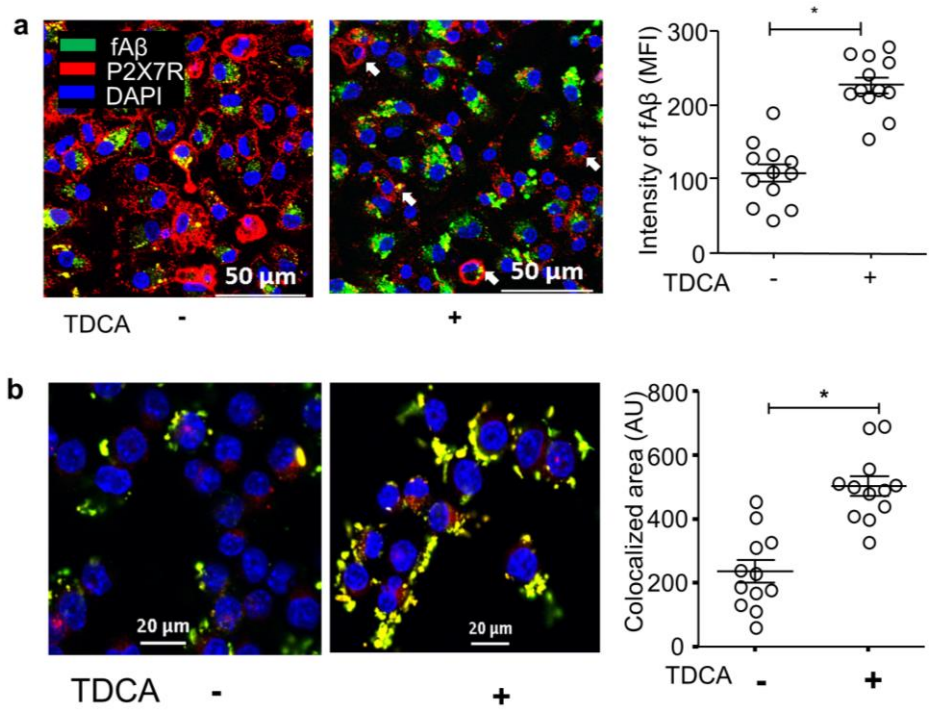

Figure 22. TDCA helps phagocytosis of Aβ by microglia.

a, The phagocytosis of fluorescent Aβ by primary microglia was determined using confocal microscopy after staining with anti-P2X7R Ab. The effects of TDCA (400 ng/ml) on phagocytosis of fAβ by BV2 cells were tested. Colocalization (yellow) of fAβ (green) with phagosomes was determined using confocal microscopy after staining with anti-LAMP2^{+}Ab (red). The area of colocalization (yellow) was quantified using ImageJ from four independent experiments (triplicate, right panel).

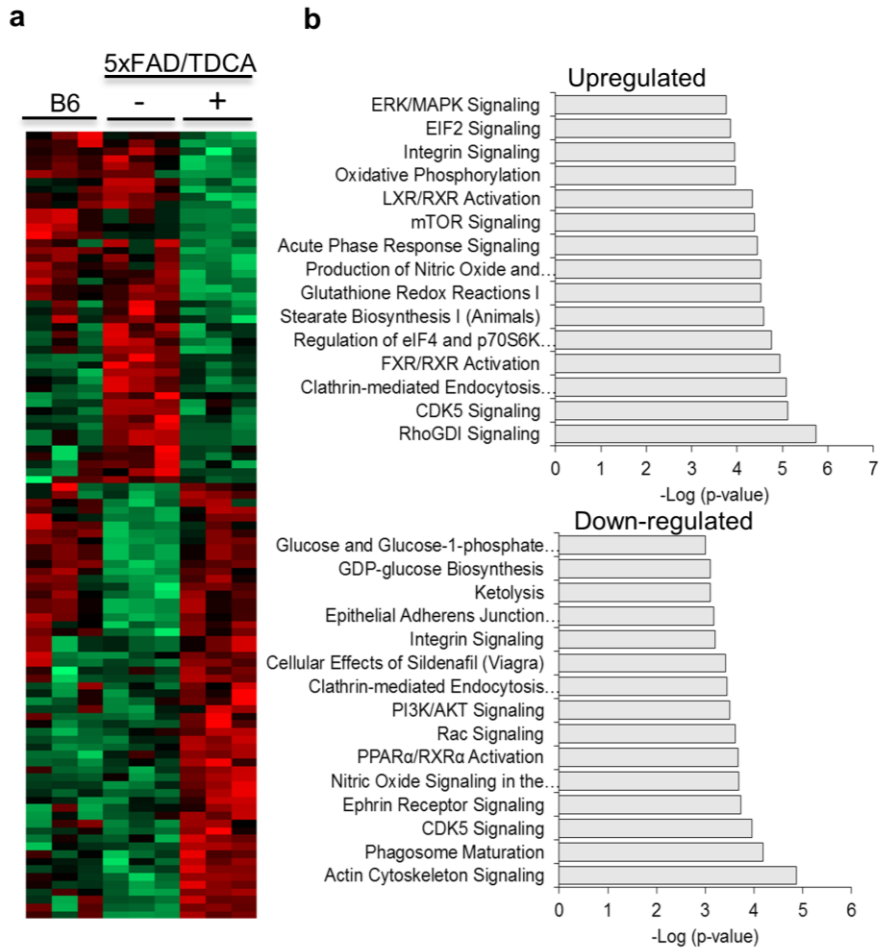

Figure 23. Proteomic analyses of mouse brains.

B6 or 5xFAD (n = 3/group) mice were treated with TDCA (1 mg/kg i.p.) for 10 weeks. **a,** Heatmap showing the differential expression of proteomes in the brain. Each row represents a protein, and each column represents an individual mouse. **b,** The top 15 canonical pathways “upregulated” or “downregulated” by treatment with TDCA are shown.

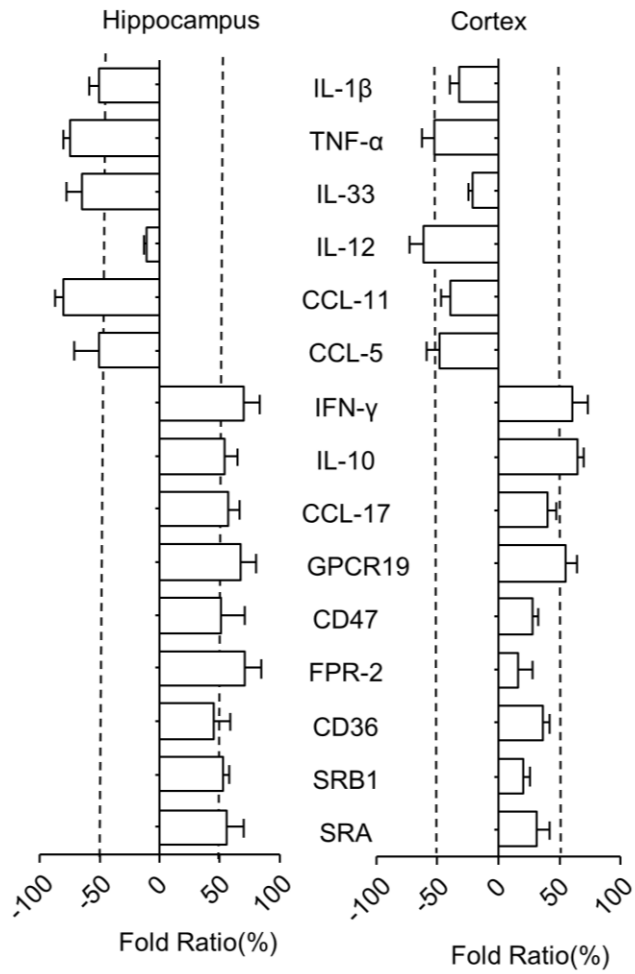

Figure 24. Gene expression of 5xFAD mouse brains.

5xFAD (n = 6/group) mice were treated with TDCA (1 mg/kg i.p.) for 10 weeks. Cytokines, chemokines, immune checkpoint molecules, and scavenger receptors expressed in the hippocampus and cortex were determined by qPCR based on proteomic profiling. Fold ratios denote the ratio between Ct_{TDCA} and $Ct_{vehicle}$. Fold ratios less than zero indicate that expression was inhibited upon TDCA treatment.

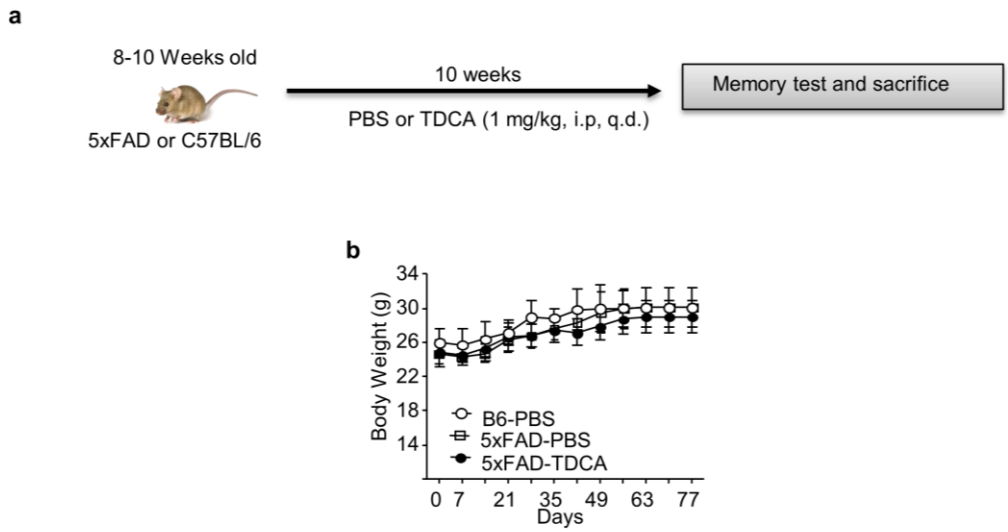

Figure 25. Schematic diagram of *in-vivo* experiments

a, A schematic diagram showing protocols of behavior tests for 5xFAD and B6 ($5xFAD^-$) mice after treatment with TDCA (1 mg/kg, i.p., q.d.) for 10 weeks. **b,** Changes in the body weight of mice are depicted.

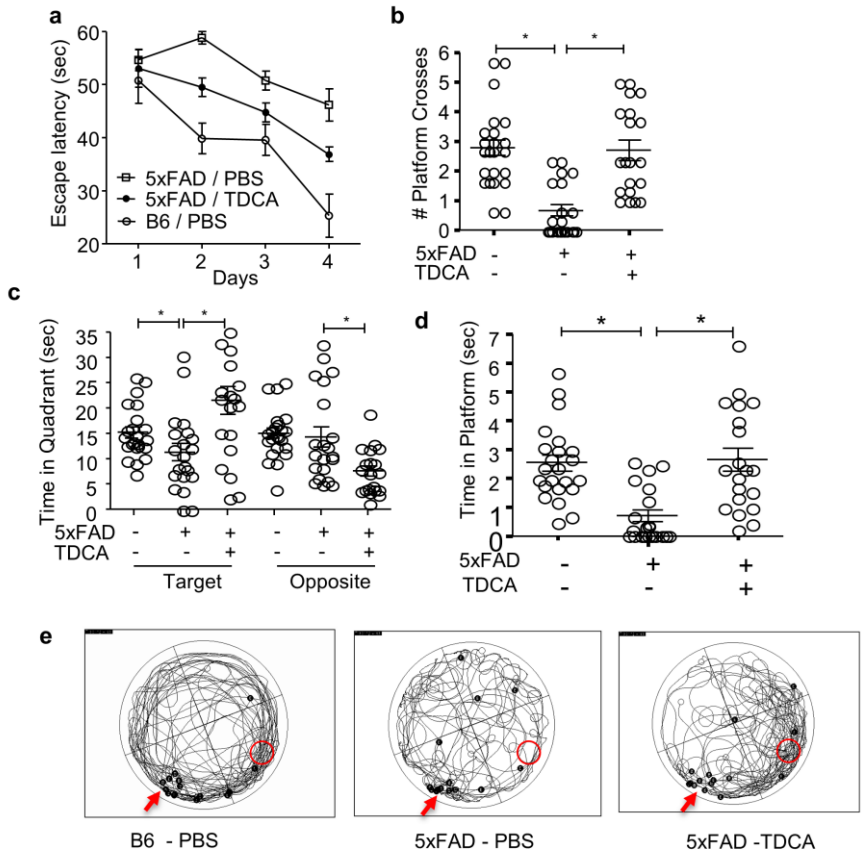

Figure 26. TDCA improves the spatial learning and memory of 5xFAD mice in the MWM test.

The learning and memory of 5xFAD and B6 ($5xFAD^-$) mice were tested after treatment with TDCA 1 mg/kg i.p. for 10 weeks (n = 20~22/group). The time to reach the hidden platform (escape latency) (**a**), the number of platform crosses (**b**) and the time spent on the target platform (**c**) were measured using the MWM test. The time spent in the target quadrant where a platform is located and the opposite quadrant (**c**) were calculated from the MWM test. **e,** Trajectory maps show the escape route of all mice in the MWM test in a set of experiments. The red arrows and red circles indicate release points and positions of the platform, respectively. Black dots indicate the beginning (B) and end (E) points for individual mice.

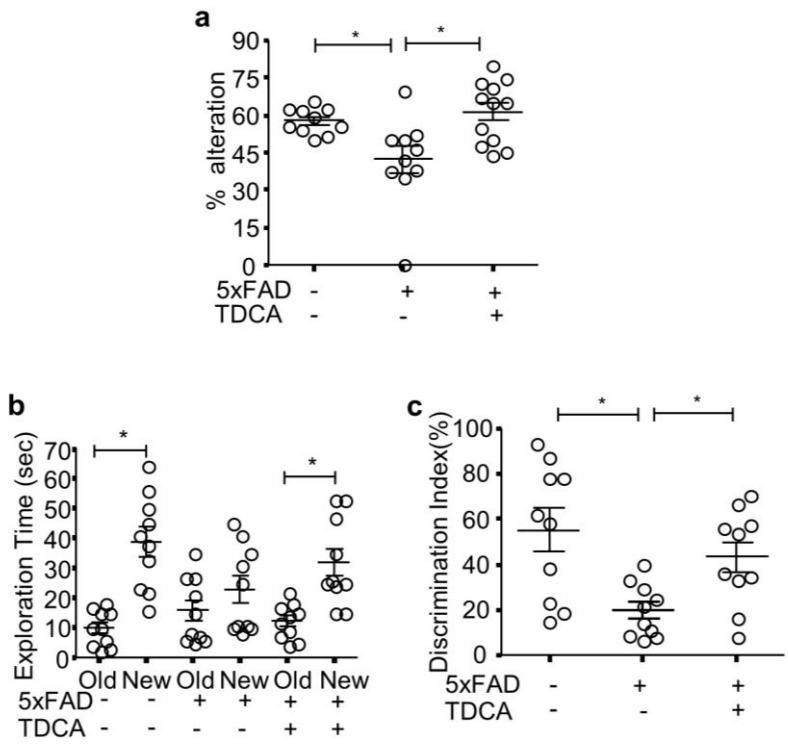

Figure 27. TDCA improves the spatial learning and memory of 5xFAD mice in the Y maze and NOR test.

The learning and memory of 5xFAD and B6 ($5xFAD^-$) mice were tested after treatment with TDCA 1 mg/kg i.p. for 10 weeks (n = 9~12/group). **a,** Alternation percentages of mice in the Y-maze test were calculated by 100 × # spontaneous alternation/# of total arm entry. **b,** Total exploration time for each object of individual mice in the NOR test is depicted. **c,** Discrimination index (%) = 100 × time spent exploring the novel object/exploration time for both the novel and old objects for each mouse (n = 10).

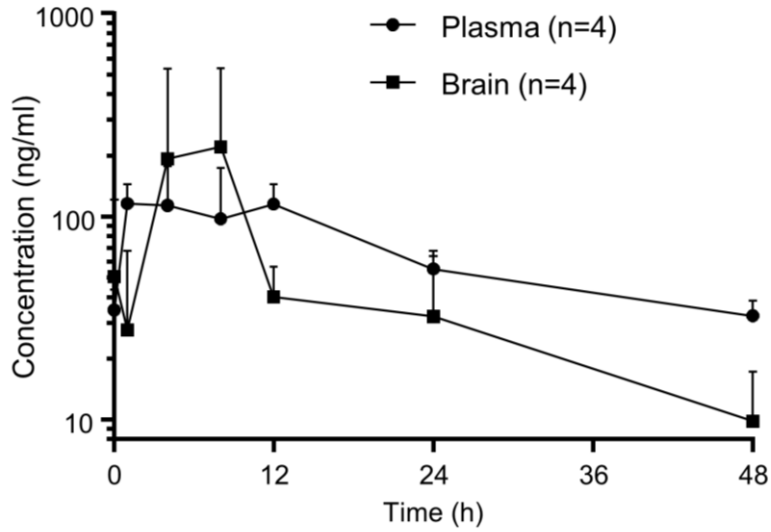

Figure 28. Pharmacokinetics of TDCA in Blood and Brain

TDCA was formulated with 0.5% CMC. PK profile of 50 mpk oral TDCA in B6 mice after a single administration was checked for different time points until 48 h.

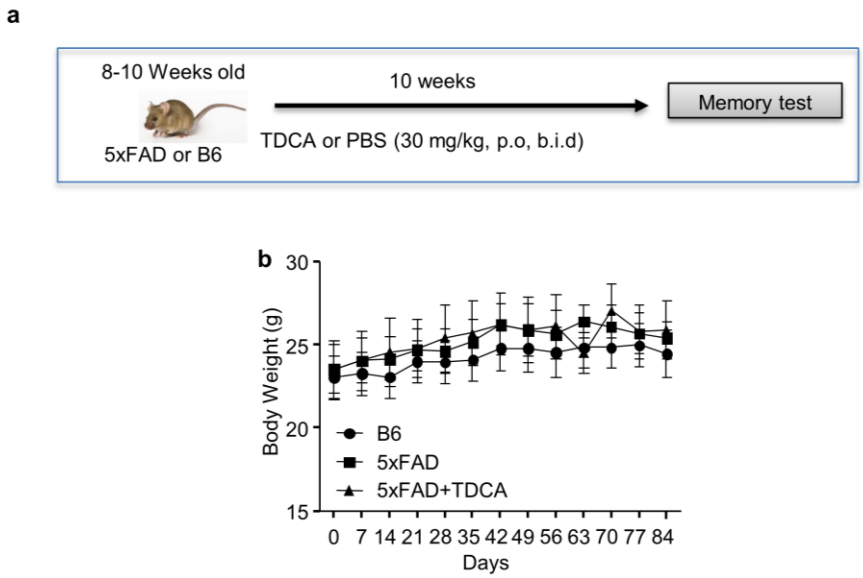

Figure 29. Schematic diagram of oral TDCA administration and *in-vivo* experiments

a, A schematic diagram showing protocols of behavior tests for 5xFAD and B6 ($5xFAD^-$) mice after treatment with TDCA (30 mg/kg, p.o., b.i.d.) for 10 weeks. **b,** Changes in the body weight of mice are depicted.

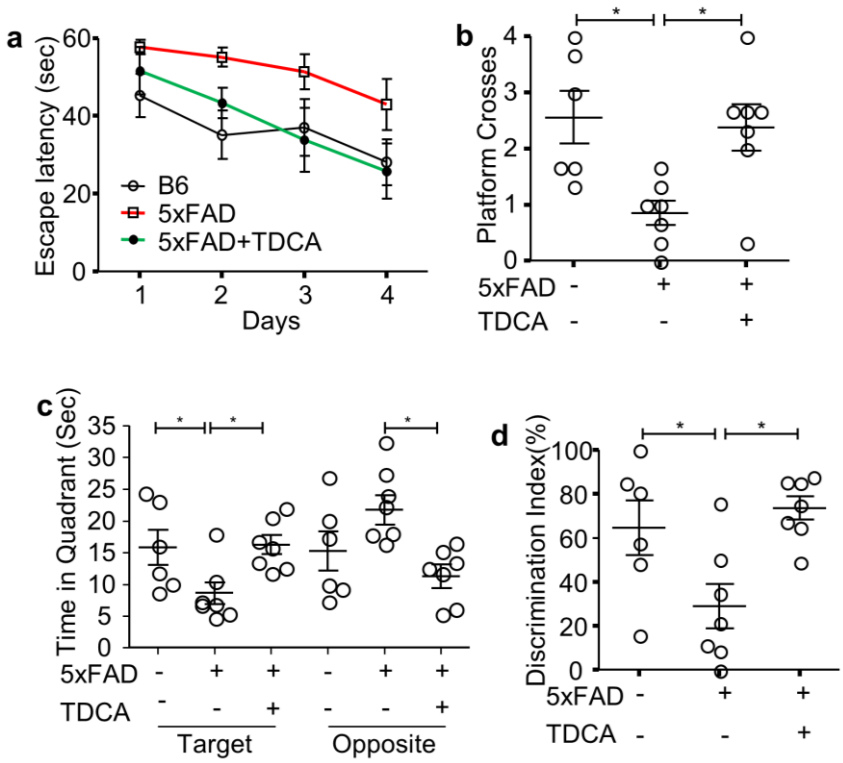

Figure 30. Oral administration of TDCA improves spatial learning and memory in 5xFAD mice.

The learning and memory of 5xFAD and B6 ($5xFAD^-$) mice were tested after treatment with TDCA 30 mg/kg p.o. for 10 weeks (n = 6~8/group). The time to reach the hidden platform (escape latency) (**a**) and the number of platform crosses (**b**) were measured using the MWM test. The time spent in the target quadrant where a platform is located and the opposite quadrant (**c**) were calculated from the MWM test. **d,** Discrimination index (%) = 100 × time spent exploring the novel object/exploration time for both the novel and old objects for each mouse.

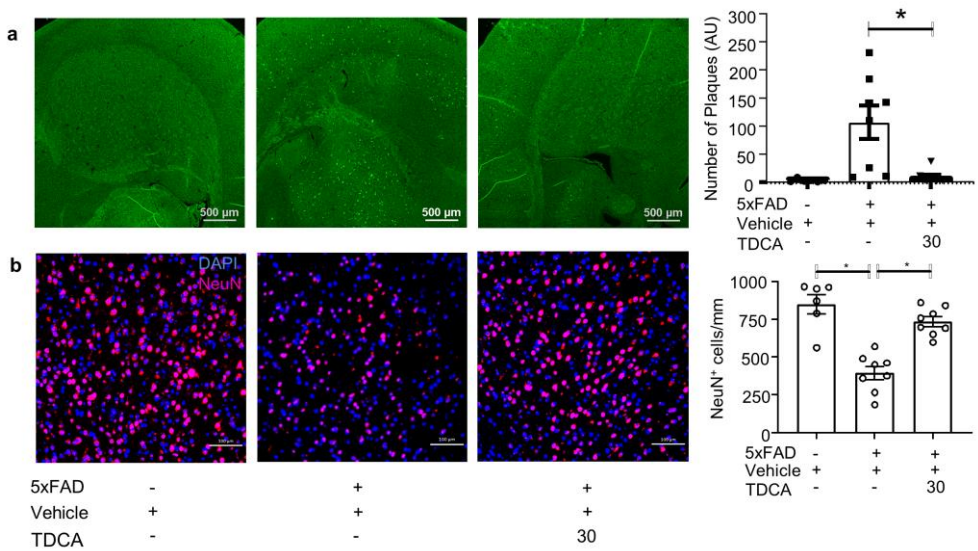

Figure 31. Oral administration of TDCA decreases Aβ plaques and apoptosis in the brains of 5xFAD mice.

a, Aβ plaques in the brain sections of 5xFAD mice administered TDCA (30 mg/kg, p.o., b.i.d.) for 10 weeks were stained with thioflavin-S (green dots indicated with white arrows). The number of plaques was quantitated using ImageJ. **b,** $NeuN^+$ cells in the cortex were analyzed using confocal microscopy. A set of representative images is depicted in the left panel, and the number of $NeuN^+$ cells is shown in the right panel.

Table 1. List of human brain tissue sections used in this study.

** NIA-AA score

KBBN ID	Gender	Age	Brain	Disease
Brains of individuals irrelevant with Alzheimer's diseases (Non-AD brains in the text)				
06006009	Male	50-59	Hippocampus	Normal (No neuritic plaque; Stage 0, B0**)
06005691	Male	60-69	Hippocampus	Normal (No neuritic plaque; Stage 0, B0**)
01000633	Female	60-69	Primary motor cortex	Interstitial lung diseases
Brains of patients with Alzheimer's diseases (AD brains in the text)				
01002998	Female	80-89	Hippocampus	Stage V, B3**
03002487	Male	80-89	Hippocampus	Stage VI, B3
05007905	Female	50-59	Brain cortex	Alzheimer's diseases neuropathological change
05007911	Male	80-89	Brain cortex	Alzheimer's diseases neuropathological change
01002964	Female	80-89	Primary motor cortex	Stage V, B3

Table 2. List of primers used in this study.

#	Gene name	Primer
1	mIL-1β-F	TTGTTGCTGTGGAGAAGCTGT
2	mIL-1β-R	AACGTCACACACCAGCAGGTT
3	mIL-12-F	GGAAGCACGGCAGCAGAATA
4	mIL-12-R	AACTTGAGGGAGAAGTAGGAATGG
5	mIL-10-F	GGTTGCCAAGCCTTATCGGA
6	mIL-10-R	ACCTGCTCCACTGCCTTGCT
7	mCD47-F	TTGCGAAGTGACAGAG TTATCC
8	mCD47-R	ACCTCCTTTCTCCTCCTCGTAA
9	mCD36-F	GAACCACTGCTTTCAAAAACTGG
10	mCD36-R	TGCTGTTCTTTGCCACGTCA
11	mSRB1-F	TTTGGAGTGGTAGT AAAAAGGGC
12	mSRB1-R	TGACATCAGGGACTCAGAGTAG
13	mIFN-γ-F	AACGCTACACACTGCATCTTGG
14	mIFN-γ-R	GCCGTGGCAGTAACAGCC
15	mTNF-α-F	AGCAAACCACCAAGTGGAGGA
16	mTNF-α-R	GCTGGCACCACTAGTTGGTTGT
17	mCCL11-F	TCCACAGCGCTTCTATTCCTG
18	mCCL11-R	GGAGCCTGGGTGAGCCA
19	mCCL17-F	CAGGGATGCCATCGTGTTTC
20	mCCL17-R	CACCAATCTGATGGCCTTCTT
21	mFPR2-F	ATTGTTGCTGTTTGCTATGGAC
22	mFPR2-R	CTGCTGTAAGGAC TCGTAAAGG
23	mSRA-F	ACATCACCAACGACCTCAGACT
24	mSRA-R	AGTTTGTCCAGTAAGC CCTCTG
25	mGAPDH-F	CAGTGGCAAAGTGGAGATTGTTG
26	mGAPDH-R	CTCGCTCCTGGAAGATGGTGAT
27	mIL-33-F	GGAGAAGGTGATGGTGAAC
28	mIL-33-R	CCACAACATCGTAAGCCAAG
29	mCCL5-F	AGATCTCTGCAGCTGCCCTCA
30	mCCL5-R	GGAGCACTTGCTGCTGGTGTAG
31	mNLRP-3-F	AGAAGAGACCACGGCAGAAG
32	mNLRP-3-R	CCTTGGACCAGGTTCAGTGT
33	mASC-F	GAGCAGCTGCAAACGACTAA
34	mASC-R	GCTGGTCCACAAAGTGTCCT
35	mPro-Caspase-1 F	GACTAAGTTGATTCCAAGCTC
36	mPro-Caspase-1 R	GATTCTGAGACCTACCTATG

Table 3: PK profile of TDCA in Blood and Brain of B6 mice

TDCA 50mpk(n=4)				
Tissue	Plasma (ng/mL)		Brain (ng/mL)	
	Mean	SD	Mean	SD
AUC (last)	3341.98	761.23	2657.64	1229.25
AUC (inf)	4368.61	579.10	2520.43	1520.83
Cmax	158.23	42.10	399.08	345.40
Tmax	4.25	2.87	11.00	8.87
t1/2	21.49	5.39	11.61	1.02
AUC 외삽%	23.95	10.17	7.06	6.70

Discussion

Senile Aβ plaques in the human brain incur microgliosis, which is responsible for neuroinflammatory cascades, causing memory and cognitive impairment, eventually progressing to dementia[10]. Reactive microgliosis accompanied by neuronal damage aggravates AD[9]. Aβ-mediated activation of N3I exacerbates the pathogenesis of AD by inducing neuroinflammation[18]. However, intervention with N3I activation to suppress neuroinflammation in AD is still not successful. Therefore, many resources have been proposed to halt the progression of Aβ-mediated N3I activation, which might delay neuronal loss due to the neuroinflammatory cascade. In this study, we found that administration of a GPCR19 agonist, TDCA (1 mg/kg, i.p., q.d. or 30 mg/kg, p.o., b.i.d.), for 10 weeks significantly improved the learning and memory of 5xFAD mice (Figure 26 and 30).

The possible mode of action of TDCA could be explained in four ways. First, TDCA suppressed the priming phase of N3I activation (transcription of NLRP3, ASC, and pro-caspase-1) (Figure 10) and the activation phase of N3I (production of mature IL-1β and IL-18 by NLRP3-ASC oligomerization) (Figure 11-14) in response to Aβ and ATP. Second, TDCA inhibited the production of crucial proinflammatory mediators, such as ROS and TNF-α, by microglia independent of N3I activation (Figures 14 and 15). Third, TDCA could augment the clearance of Aβ by enhancing phagocytosis through increasing SRA expression (Figure 21) and suppressing P2X7 expression (Figure 22). Overall, TDCA reduces neuroinflammation and prevents neuronal apoptosis (Figures 16, 17 and 31), which delays the impairment of spatial learning and memory (Figures 26 and 30).

TDCA regulates N3I activation by altering the functions and expression of P2X7R after binding with GPCR19 (Figure 5). The P2X7R on microglia is crucial in Ca^{++} mobilization that initiates N3I activation[65]. Many glial functions are mediated by

Ca^{++}[34], such as the production of cytokines and chemokines[66]. ATP released from damaged neurons could activate P2X7R in AD.

Upon stimulation with P2X7R agonists (ATP or BzATP), $GPCR19^{-/-}$ microglia could not mobilize cytosolic Ca^{++} as much as WT microglia (Figure 7), suggesting that GPCR19 is a prerequisite in Ca^{++} mobilization in response to P2X7R agonists within 100 sec. ATP enables the open state of P2X7R on the cell membrane, thereby encouraging the exchange of cytosolic and extracellular cations[67]. The crystal structure of the P2X7 receptor displays clear differences between the open and closed pore states[68]. However, no studies have reported the role of GPCR19 in this process until now. Several findings in this study suggest the biphasic role of GPCR19 in regulating P2X7R. In the immediate phase in response to proinflammatory cues such as Aβ and/or ATP (50 – 150 sec), TDCA may regulate the function of P2X7R by allosteric modulation of GPCR19, which interferes with the GPCR19-P2X7R interaction. GPCR19 and P2X7R are colocalized on the cell membrane of resting microglia (Figure 1), and Ca^{++} is mobilized within 100 sec in response to ATP. A GPCR19 agonist, TDCA, inhibited Ca^{++} mobilization when microglia were stimulated with Aβ + P2X7R agonist (ATP or BzATP) within 100 sec, further supporting the idea that GPCR19 is a prerequisite for the activation of P2X7R and TDCA interferes with the interaction of these two molecules (Figure 8 and 9). This finding suggests that the binding of TDCA with GPCR19 might cis-regulate the opening of the pore of P2X7R. It is supposed that the binding of TDCA with GPCR19 might alter the tertiary structure of GPCR19 necessary for opening the pore of P2X7R in response to its ligands. In the delayed phase in response to Aβ and/or ATP (1 h), TDCA suppresses P2X7R expression and increases the expression of GPCR19 on the cell membrane (Figure 5), suggesting plausible trans-regulation of P2X7R expression by the GPCR19-mediated signaling cascade. In summary, the TDCA-GPCR19 complex might transmit signals necessary for

inhibiting P2X7R expression on the membrane within an hour (delayed response) and might alter the structures of GPCR19 necessary for the Ca^{++} current incurred by P2X7R activation within a couple of seconds (immediate response).

In the brains of nine-month-old 5xFAD mice, the expression of GPCR19 was significantly lower and the expression of P2X7R was significantly higher than levels observed in the brains of three-month-old 5xFAD mice or B6 mice (Figure 3). The expression levels of GPCR19 and P2X7R on microglia were reciprocally regulated after stimulation with Aβ ± ATP *in vitro*, which was reversed by TDCA treatment (Figure 5). Taken together, these findings suggest that neuroinflammation induced by Aβ might be responsible for the downregulation of anti-inflammatory GPCR19 and the upregulation of proinflammatory P2X7R upon aging. The relative expression levels of GPCR19 and P2X7R on microglia might be crucial biomarkers indicating the severity of neuroinflammation in AD patients.

P2X7R inhibits phagocytosis of Aβ in various proinflammatory microenvironments in AD[39]. TDCA enhanced phagocytosis of Aβ and coincided with downregulation of P2X7R expression in microglia (Figure 22). Downregulation of P2X7R, which inhibits phagocytosis and enhances phagocytosis, might explain the possible roles of TDCA in clearing Aβ plaques in the brains of 5xFAD mice *in vivo* (Figure 20).

Proteomic analysis supports these ideas. Whole-brain lysates exhibited global editing of the brain proteome that led to an anti-inflammatory microenvironment in the AD brain (Figure 23a). For example, upregulation of clathrin-mediated endocytosis, FXR pathway, mTOR signaling, and acute phase response signaling, in addition to downregulation of NO signaling and PI3K/AKT signaling, were observed after treatment with TDCA (Figure 23b).

Various bile acids are GPCR19 agonists and can reduce inflammation in the brain[51]. However, many studies have been carried out with bile acids at concentrations that

are unobtainable under pharmacological or pathological conditions *in vivo*[69]. Thus, the exact role of bile acids in modulating brain inflammation in AD could not be concluded. In this study, we showed that TDCA, one of the bile acids interacting with GPCR19[52], could suppress brain inflammation in 5xFAD mice by inhibiting the P2X7R-N3I axis. Furthermore, oral administration of TDCA also improved spatial learning and memory, as observed with i.p. injection of TDCA. Considering the safety profiles of TDCA after i.v. administration[70], TDCA may provide a viable option for AD patients to ameliorate neuroinflammation that might delay the progression of AD.

References

1. Cunningham, E.L., McGuinness, B., Herron, B. & Passmore, A.P. Dementia. *Ulster Med J* **84**, 79-87 (2015).
2. Huang, Y. & Mucke, L. Alzheimer mechanisms and therapeutic strategies. *Cell* **148**, 1204-1222 (2012).
3. Marco A. Meraz-Ríos, D.T.-R., Diana Franco-Bocanegra, Juana Villeda-Hernández and Victoria Campos-Peña. Inflammatory process in Alzheimer's Disease. *Frontiers in Integrative Neuroscience* **7**(2013).
4. Barage, S.H. & Sonawane, K.D. Amyloid cascade hypothesis: Pathogenesis and therapeutic strategies in Alzheimer's disease. *Neuropeptides* (2015).
5. Mondragon-Rodriguez, S., Perry, G., Zhu, X. & Boehm, J. Amyloid Beta and tau proteins as therapeutic targets for Alzheimer's disease treatment: rethinking the current strategy. *Int J Alzheimers Dis* **2012**, 630182 (2012).
6. Kametani, F. & Hasegawa, M. Reconsideration of Amyloid Hypothesis and Tau Hypothesis in Alzheimer's Disease. *Front Neurosci* **12**, 25 (2018).
7. Raschetti, R., Albanese, E., Vanacore, N. & Maggini, M. Cholinesterase inhibitors in mild cognitive impairment: a systematic review of randomised trials. *PLoS Med* **4**, e338 (2007).
8. Nirzhor, S.S.R., Khan, R.I. & Neelotpol, S. The Biology of Glial Cells and Their Complex Roles in Alzheimer's Disease: New Opportunities in Therapy. *Biomolecules* **8**(2018).
9. Hickman, S.E., Allison, E.K. & El Khoury, J. Microglial dysfunction and defective beta-amyloid clearance pathways in aging Alzheimer's disease mice. *J Neurosci* **28**, 8354-8360 (2008).
10. Hardy, J. & Higgins, G. Alzheimer's disease: the amyloid cascade hypothesis. *Science* **256**, 184-185 (1992).
11. Kinney, J.W.*, et al.* Inflammation as a central mechanism in Alzheimer's disease. *Alzheimers Dement (N Y)* **4**, 575-590 (2018).
12. Kocahan, S. & Dogan, Z. Mechanisms of Alzheimer's Disease Pathogenesis and Prevention: The Brain, Neural Pathology, N-methyl-D-aspartate Receptors, Tau Protein and Other Risk Factors. *Clin Psychopharmacol Neurosci* **15**, 1-8 (2017).

13. Seong, S.Y. & Matzinger, P. Hydrophobicity: an ancient damage-associated molecular pattern that initiates innate immune responses. *Nat Rev Immunol* **4**, 469-478 (2004).
14. Zotova, E., Nicoll, J.A., Kalaria, R., Holmes, C. & Boche, D. Inflammation in Alzheimer's disease: relevance to pathogenesis and therapy. *Alzheimers Res Ther* **2**, 1 (2010).
15. Ardura-Fabregat, A.*, et al.* Targeting Neuroinflammation to Treat Alzheimer's Disease. *CNS Drugs* **31**, 1057-1082 (2017).
16. Guo, H., Callaway, J.B. & Ting, J.P. Inflammasomes: mechanism of action, role in disease, and therapeutics. *Nat Med* **21**, 677-687 (2015).
17. Heneka, M.T.*, et al.* NLRP3 is activated in Alzheimer's disease and contributes to pathology in APP/PS1 mice. *Nature* **493**, 674-678 (2013).
18. Tan, M.S.*, et al.* NLRP3 polymorphisms are associated with late-onset Alzheimer's disease in Han Chinese. *J Neuroimmunol* **265**, 91-95 (2013).
19. Dempsey, C.*, et al.* Inhibiting the NLRP3 inflammasome with MCC950 promotes non-phlogistic clearance of amyloid-β and cognitive function in APP/PS1 mice. *Brain Behav Immun* **61**, 306-316 (2017).
20. Tan, M.S., Yu, J.T., Jiang, T., Zhu, X.C. & Tan, L. The NLRP3 inflammasome in Alzheimer's disease. *Mol Neurobiol* **48**, 875-882 (2013).
21. Sheedy, F.J.*, et al.* CD36 coordinates NLRP3 inflammasome activation by facilitating intracellular nucleation of soluble ligands into particulate ligands in sterile inflammation. *Nat Immunol* **14**, 812-820 (2013).
22. Mehta, D., Jackson, R., Paul, G., Shi, J. & Sabbagh, M. Why do trials for Alzheimer's disease drugs keep failing? A discontinued drug perspective for 2010-2015. *Expert Opin Investig Drugs* **26**, 735-739 (2017).
23. Broz, P. & Dixit, V.M. Inflammasomes: mechanism of assembly, regulation and signalling. *Nat Rev Immunol* **16**, 407-420 (2016).
24. Kerur, N.*, et al.* IFI16 acts as a nuclear pathogen sensor to induce the inflammasome in response to Kaposi Sarcoma-associated herpesvirus infection. *Cell Host Microbe* **9**, 363-375 (2011).
25. Dong, Y., Li, X., Cheng, J. & Hou, L. Drug Development for Alzheimer's Disease: Microglia Induced Neuroinflammation as a Target? *Int J Mol Sci* **20**(2019).
26. Dempsey, C.*, et al.* Inhibiting the NLRP3 inflammasome with MCC950 promotes non-phlogistic clearance of amyloid-beta and cognitive function in APP/PS1 mice. *Brain, behavior, and immunity* **61**, 306-316

(2017).

27. Rathinam, V.A.K. & Chan, F.K. Inflammasome, Inflammation, and Tissue Homeostasis. *Trends Mol Med* **24**, 304-318 (2018).
28. He, Y., Hara, H. & Núñez, G. Mechanism and Regulation of NLRP3 Inflammasome Activation. *Trends Biochem Sci* **41**, 1012-1021 (2016).
29. Burnstock, G. Purinergic Signalling and Neurological Diseases: An Update. *CNS Neurol Disord Drug Targets* **16**, 257-265 (2017).
30. Saez-Orellana, F.*, et al.* P2X receptor overexpression induced by soluble oligomers of amyloid beta peptide potentiates synaptic failure and neuronal dyshomeostasis in cellular models of Alzheimer's disease. *Neuropharmacology* **128**, 366-378 (2018).
31. Abbracchio, M.P., Burnstock, G., Verkhratsky, A. & Zimmermann, H. Purinergic signalling in the nervous system: an overview. *Trends Neurosci* **32**, 19-29 (2009).
32. Sanz, J.M.*, et al.* Activation of microglia by amyloid {beta} requires P2X7 receptor expression. *J Immunol* **182**, 4378-4385 (2009).
33. Karmakar, M., Katsnelson, M.A., Dubyak, G.R. & Pearlman, E. Neutrophil P2X7 receptors mediate NLRP3 inflammasome-dependent IL-1beta secretion in response to ATP. *Nat Commun* **7**, 10555 (2016).
34. McLarnon, J.G., Ryu, J.K., Walker, D.G. & Choi, H.B. Upregulated expression of purinergic P2X(7) receptor in Alzheimer disease and amyloid-beta peptide-treated microglia and in peptide-injected rat hippocampus. *J Neuropathol Exp Neurol* **65**, 1090-1097 (2006).
35. Kelley, N., Jeltema, D., Duan, Y. & He, Y. The NLRP3 Inflammasome: An Overview of Mechanisms of Activation and Regulation. *Int J Mol Sci* **20**(2019).
36. Delekate, A.*, et al.* Metabotropic P2Y1 receptor signalling mediates astrocytic hyperactivity in vivo in an Alzheimer's disease mouse model. *Nat Commun* **5**, 5422 (2014).
37. Gong, T., Liu, L., Jiang, W. & Zhou, R. DAMP-sensing receptors in sterile inflammation and inflammatory diseases. *Nat Rev Immunol* **20**, 95-112 (2020).
38. Kim, S.Y., Moon, J.H., Lee, H.G., Kim, S.U. & Lee, Y.B. ATP released from beta-amyloid-stimulated microglia induces reactive oxygen species production in an autocrine fashion. *Exp Mol Med* **39**, 820-827 (2007).
39. Gu, B.J. & Wiley, J.S. P2X7 as a scavenger receptor for innate

phagocytosis in the brain. *Br J Pharmacol* **175**, 4195-4208 (2018).

40. Ni, J., Wang, P., Zhang, J., Chen, W. & Gu, L. Silencing of the P2X(7) receptor enhances amyloid-beta phagocytosis by microglia. *Biochem Biophys Res Commun* **434**, 363-369 (2013).
41. Martin, E.*, et al.* New role of P2X7 receptor in an Alzheimer's disease mouse model. *Mol Psychiatry* **24**, 108-125 (2019).
42. Albalawi, F.*, et al.* The P2X7 Receptor Primes IL-1beta and the NLRP3 Inflammasome in Astrocytes Exposed to Mechanical Strain. *Front Cell Neurosci* **11**, 227 (2017).
43. Nizami, S., Hall-Roberts, H., Warrier, S., Cowley, S.A. & Di Daniel, E. Microglial inflammation and phagocytosis in Alzheimer's disease: Potential therapeutic targets. *Br J Pharmacol* **176**, 3515-3532 (2019).
44. Thawkar, B.S. & Kaur, G. Inhibitors of NF-κB and P2X7/NLRP3/Caspase 1 pathway in microglia: Novel therapeutic opportunities in neuroinflammation induced early-stage Alzheimer's disease. *J Neuroimmunol* **326**, 62-74 (2019).
45. Bartlett, R., Stokes, L. & Sluyter, R. The P2X7 receptor channel: recent developments and the use of P2X7 antagonists in models of disease. *Pharmacol Rev* **66**, 638-675 (2014).
46. Evangelakos, I., Heeren, J., Verkade, E. & Kuipers, F. Role of bile acids in inflammatory liver diseases. *Semin Immunopathol* **43**, 577-590 (2021).
47. Mangelsdorf, D.J.*, et al.* The nuclear receptor superfamily: the second decade. *Cell* **83**, 835-839 (1995).
48. Suga, T.*, et al.* Preference of Conjugated Bile Acids over Unconjugated Bile Acids as Substrates for OATP1B1 and OATP1B3. *PLoS One* **12**, e0169719 (2017).
49. Copple, B.L. & Li, T. Pharmacology of bile acid receptors: Evolution of bile acids from simple detergents to complex signaling molecules. *Pharmacol Res* **104**, 9-21 (2016).
50. Guo, C.*, et al.* The G-Protein-Coupled Bile Acid Receptor Gpbar1 (TGR5) Inhibits Gastric Inflammation Through Antagonizing NF-κB Signaling Pathway. *Front Pharmacol* **6**, 287 (2015).
51. McMillin, M.*, et al.* TGR5 signaling reduces neuroinflammation during hepatic encephalopathy. *J Neurochem* **135**, 565-576 (2015).
52. Wan, Y.Y. & Sheng, L. Regulation of bile acid receptor activity(☆). *Liver Res* **2**, 180-185 (2018).

53. Jia, W., Wei, M., Rajani, C. & Zheng, X. Targeting the alternative bile acid synthetic pathway for metabolic diseases. *Protein Cell* **12**, 411-425 (2021).
54. Carino, A.*, et al.* Ursodeoxycholic acid is a GPBAR1 agonist and resets liver/intestinal FXR signaling in a model of diet-induced dysbiosis and NASH. *Biochim Biophys Acta Mol Cell Biol Lipids* **1864**, 1422-1437 (2019).
55. Elia, A.E.*, et al.* Tauroursodeoxycholic acid in the treatment of patients with amyotrophic lateral sclerosis. *Eur J Neurol* **23**, 45-52 (2016).
56. Yanguas-Casás, N., Barreda-Manso, M.A., Nieto-Sampedro, M. & Romero-Ramírez, L. TUDCA: An Agonist of the Bile Acid Receptor GPBAR1/TGR5 With Anti-Inflammatory Effects in Microglial Cells. *J Cell Physiol* **232**, 2231-2245 (2017).
57. Kumar, D.P.*, et al.* Activation of Transmembrane Bile Acid Receptor TGR5 Modulates Pancreatic Islet α Cells to Promote Glucose Homeostasis. *J Biol Chem* **291**, 6626-6640 (2016).
58. Jin, P.*, et al.* INT-777 prevents cognitive impairment by activating Takeda G protein-coupled receptor 5 (TGR5) and attenuating neuroinflammation via cAMP/ PKA/ CREB signaling axis in a rat model of sepsis. *Exp Neurol* **335**, 113504 (2021).
59. Thomas, C.*, et al.* TGR5-mediated bile acid sensing controls glucose homeostasis. *Cell Metab* **10**, 167-177 (2009).
60. Pols, T.W.*, et al.* TGR5 activation inhibits atherosclerosis by reducing macrophage inflammation and lipid loading. *Cell Metab* **14**, 747-757 (2011).
61. Biagioli, M.*, et al.* The Bile Acid Receptor GPBAR1 Regulates the M1/M2 Phenotype of Intestinal Macrophages and Activation of GPBAR1 Rescues Mice from Murine Colitis. *J Immunol* **199**, 718-733 (2017).
62. Liang, H.*, et al.* TGR5 activation attenuates neuroinflammation via Pellino3 inhibition of caspase-8/NLRP3 after middle cerebral artery occlusion in rats. *J Neuroinflammation* **18**, 40 (2021).
63. Oakley, H.*, et al.* Intraneuronal beta-amyloid aggregates, neurodegeneration, and neuron loss in transgenic mice with five familial Alzheimer's disease mutations: potential factors in amyloid plaque formation. *J Neurosci* **26**, 10129-10140 (2006).
64. Kersey, P.J.*, et al.* The International Protein Index: an integrated database

for proteomics experiments. *Proteomics* **4**, 1985-1988 (2004).

65. Liu, Y.-H*., et al.* The ATP-P2X7 Signaling Axis Is an Essential Sentinel for Intracellular Clostridium difficile Pathogen-Induced Inflammasome Activation. *Frontiers in Cellular and Infection Microbiology* **8**(2018).
66. Hoffmann, A., Kann, O., Ohlemeyer, C., Hanisch, U.K. & Kettenmann, H. Elevation of basal intracellular calcium as a central element in the activation of brain macrophages (microglia): suppression of receptor-evoked calcium signaling and control of release function. *J Neurosci* **23**, 4410-4419 (2003).
67. Khakh, B.S. & North, R.A. Neuromodulation by extracellular ATP and P2X receptors in the CNS. *Neuron* **76**, 51-69 (2012).
68. Karasawa, A. & Kawate, T. Expression and Purification of a Mammalian P2X7 Receptor from Sf9 Insect Cells. *Bio Protoc* **7**(2017).
69. Guo, C*., et al.* Bile Acids Control Inflammation and Metabolic Disorder through Inhibition of NLRP3 Inflammasome. *Immunity* **45**, 802-816 (2016).
70. Choi, H.J*., et al.* Nonclinical toxicology studies with sodium taurodeoxycholate: acute and subacute toxicity in dogs. *Drug Chem Toxicol*, 1-9 (2019).

Abstract in Korean (초록)

알츠하이머병(AD)은 신경 퇴행성 뇌질환으로, 신경반(neuritic plaque)과 신경섬유다발(neurofibrillary tangle)에 의한 염증이 주요 병인 기전이다. 아밀로이드 베타(Aβ)에 의해 유발된 신경염증은 NLRP3 인프라마좀(N3I)을 활성화시킴으로써 신경 세포의 자살 (Apoptosis)을 유발한다. 본 연구에서 G단백질 연결 수용체 19 (GPCR19) 작용제인 타우로데옥시콜레이트 (TDCA)가 신경 염증과 신경 퇴행을 억제함을 관찰하였다.

미세아교세포의 P2X7R에 의한 NLRP3 인프라마좀의 활성화는 알츠하이머병(AD)의 신경 염증반응에 중요한 기전이다. 아밀로이드 베타(Aβ) 및 ATP와 같은 손상연관분자패턴(DAMP)는 P2X7R 경로를 통해 N3I를 활성화시킨다.
GPCR19는 미세아교세포를 포함한 골수성 면역 세포(myeloid immune cells)에서 많이 발현된다. GPCR19는 미세아교세포의 막에 P2X7R와 함께 존재하며, P2X7R을 매개로 하는 N3I의 활성화를 조절함을 관찰하였다. 알츠하이머 형 마우스(5xFAD) 모델에서, GPCR19 및 P2X7R 발현은 노화진행에 따라 변화하였다. TDCA는 일정상마우스에서 IL-1β 생산을 억제했지만, GPCR19KO 및 P2X7RKO 미세아교세포에서는 억제하지 않았다. 미세아교세포에서 ATP 또는 BzATP에 의한 Ca^{++} 이동(mobilization)은 정상 세포와 비교했을 때 GPCR19KO 및 P2X7RKO 세포에서 감소하였다. 이는 GPCR19가 P2X7R을 매개로 하는N3I 활성화를 통해 IL-1β/IL-18의 생산에 중요한 역할을 한다는 것을 보여준다. 시험관 실험에서 TDCA는 Aβ±ATP에 의한 미세아교세포의 NLRP3-ASC 복합체 형성과IL-1β/IL-18 성숙을 억제하였고, TDCA는 GPCR19-cAMP-PKA-NF-kB 경로를 통하여 N3I 활성화의 개시 단계를 억제시키는 것을 확인하였다.

10주 동안 TDCA(1mg/kg)를 1일1회 복강내 주사하였을 때, 5xFAD 마우스의 대뇌피질에서 P2X7R의 발현을 억제하고, Aβ의 대식작용를 향상시키고, Aβ 플라그의 수를 감소시켰다. 또한, TDCA는 미세아교세포의 비정상적인 숫적 증가를 감소시켰으며, 신경손실을 방지하였고, 5xFAD 마우스의 인지.기억 능력을 향상시켰다. 뿐만 아니라, 10주동안 TDCA(30mg/kg)를 1일2회 경구투여 하였을 때도, 5xFAD 마우스의 인지.기억 기능을 향상시켰다. 단일 경구 투여 후, 혈장 및 뇌에서 TDCA의 AUC(last)는 각각 3341.98ng/ml 및 2657.64ng/ml이며, 이는 뇌로의 TDCA 분포를 보여준다. 따라서, P2X7R을 통한 N3I 활성화에 있어서 GPCR19의 다양한 역할을 고려할때 GPCR19를 표적으로 하는 치료제는 AD 환자의 인지.기억능 향상에 기여 할수있을것으로 사료된다.